Pourquoi le MEB bas voltage peut-il compétitionner avec le MET conventionnel ?

Pr. Raynald Gauvin, Ph.D.
Nicolas Brodusch, M.Sc.A
Stéphanie Bessette, M.Sc.A

McGill

Montréal, Québec, Canada.

TEM Resolution vs Time

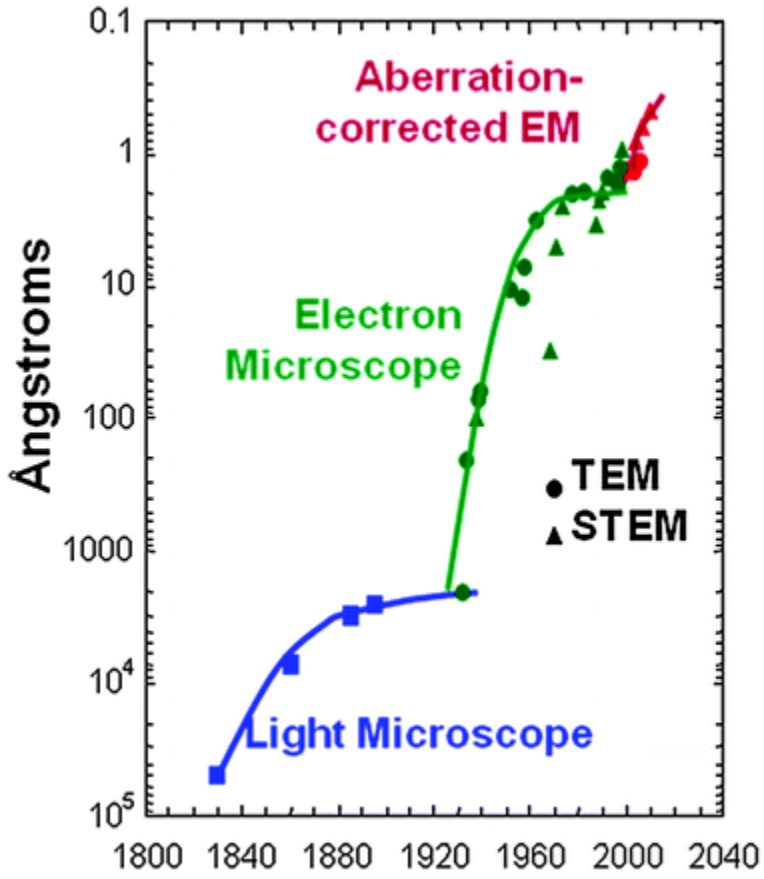

Si_6 Cluster in Graphene

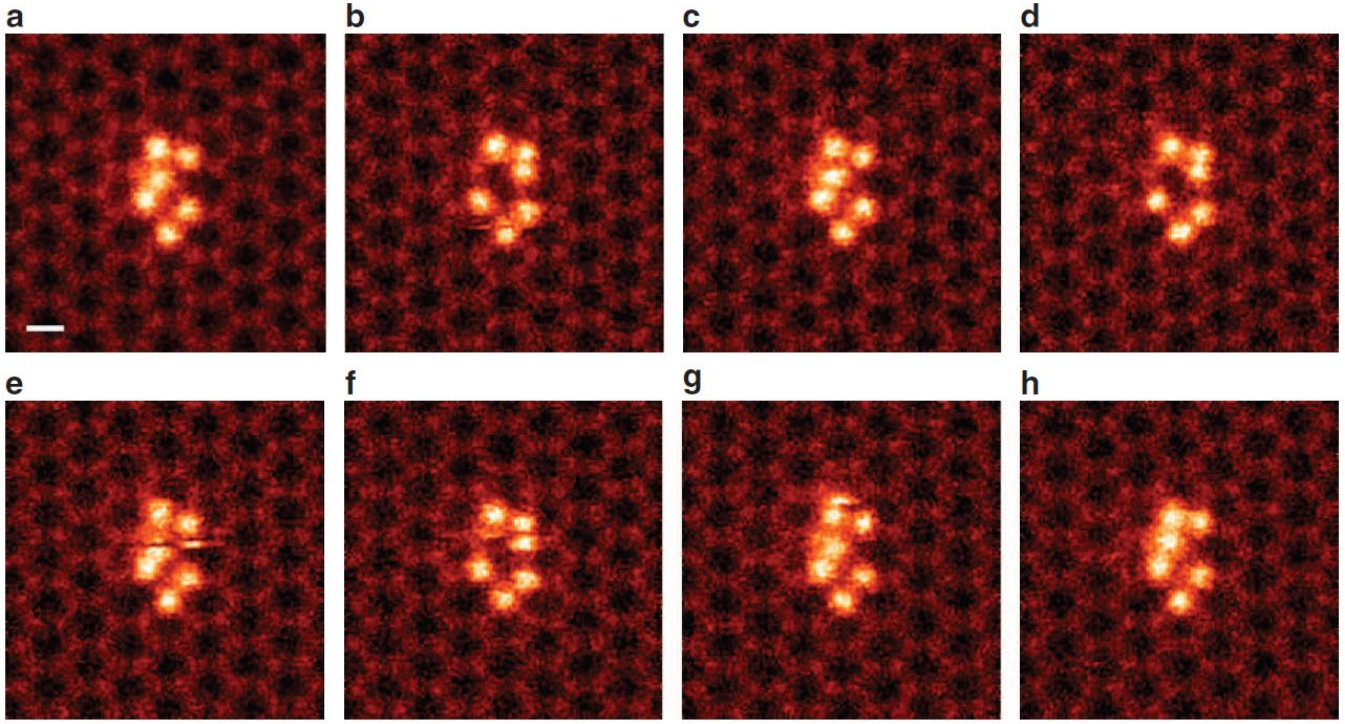

Figure 1 | Sequential STEM-ADF Z-contrast images of the Si_6 cluster embedded in a graphene pore (**a**–**h**) The images have been low-pass filtered in order to reduce random noise. Scale bar, 0.2 nm.

Lee, J.; Zhou, W.; Pennycook, S. J.; Idrobo, J.-C.; Pantelides, S. T. Direct Visualization of Reversible Dynamics in a Si6 Cluster Embedded in a Graphene Pore. Nature Communications 2013, 4, 1650–7.

TEM/STEM Modernes

Très dispendueux !!!

Nombre limité !!!

Que peut-on faire ????

CASINO

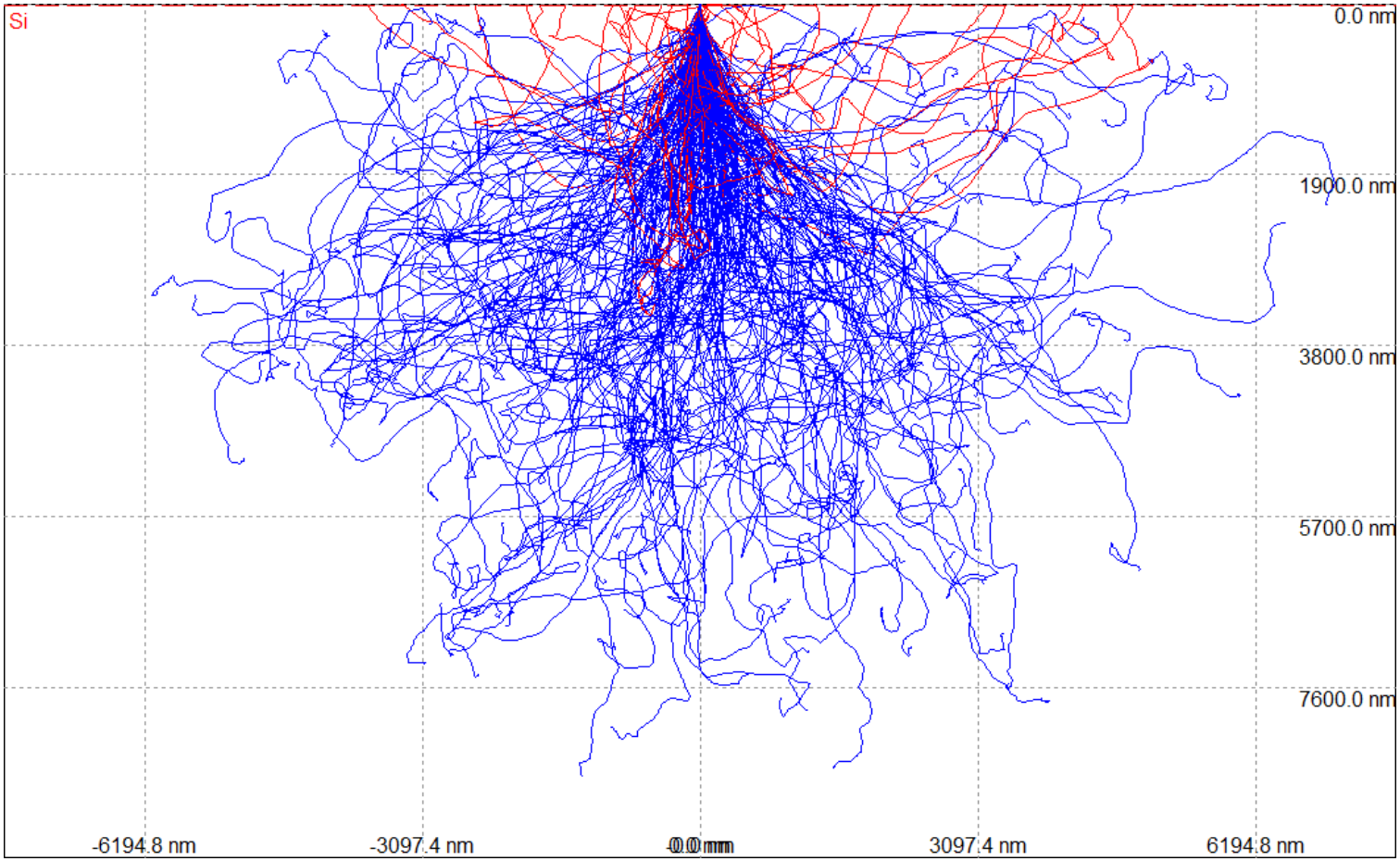

CASINO: A new Monte Carlo code in C language for electron beam interaction .1. Description of the program
By: Hovington, P; Drouin, D; Gauvin, R
SCANNING Volume: 19 Issue: 1 Pages: 1-14 Published: JAN 1997 **795 Citations Google Scholar (26/11/22)**

CASINO V2.42 - A fast and easy-to-use modeling tool for scanning electron microscopy and microanalysis users
By: Drouin, D.; Couture, A. R.; Joly, D. and Gauvin, R.
SCANNING Volume: 29 Issue: 3 Pages: 92-101 Published: MAY-JUN 2007 **1590 Citations Google Scholar (26/11/22)**

Low Voltage SEM

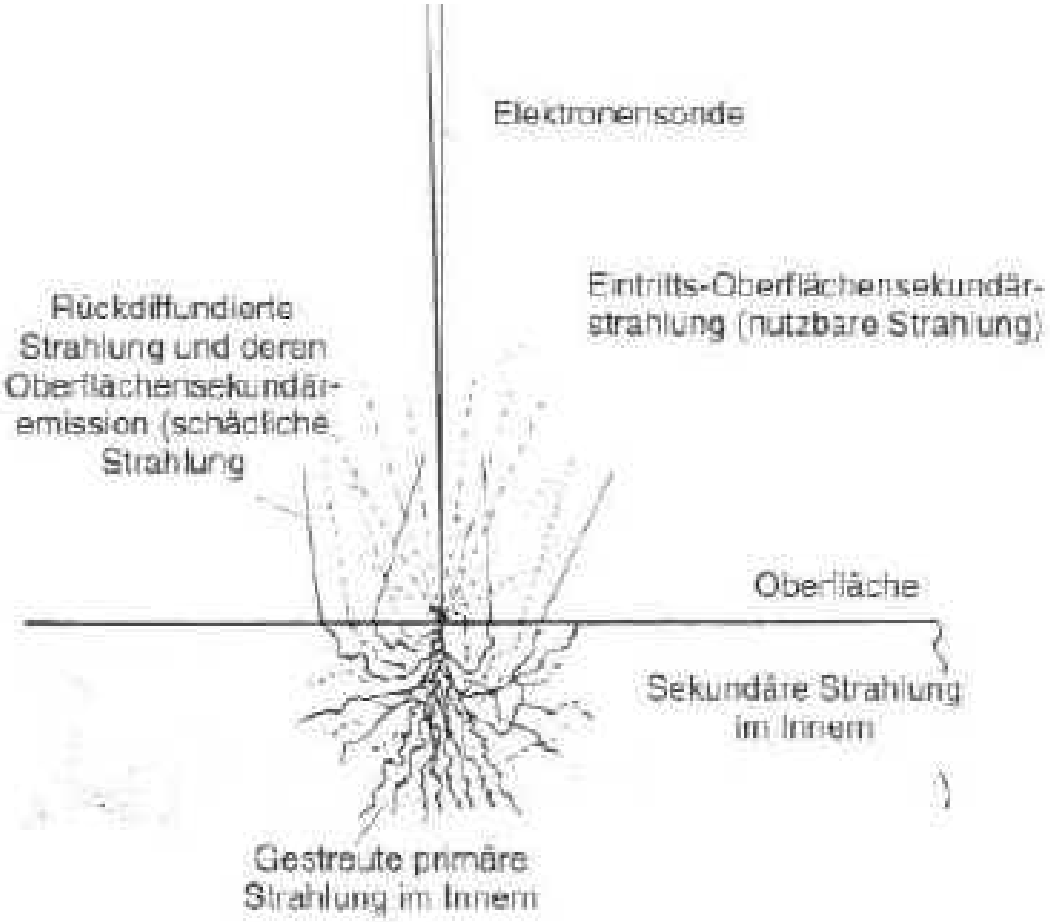

FIG. 6 Diagram illustrating von Ardenne's (1940) discussion of secondary electron imaging of a surface.

- Small interaction volume
- Improved spatial resolution

Von Ardenne 1940

Monte Carlo Simulations
10 nm MnS Inclusion in Fe

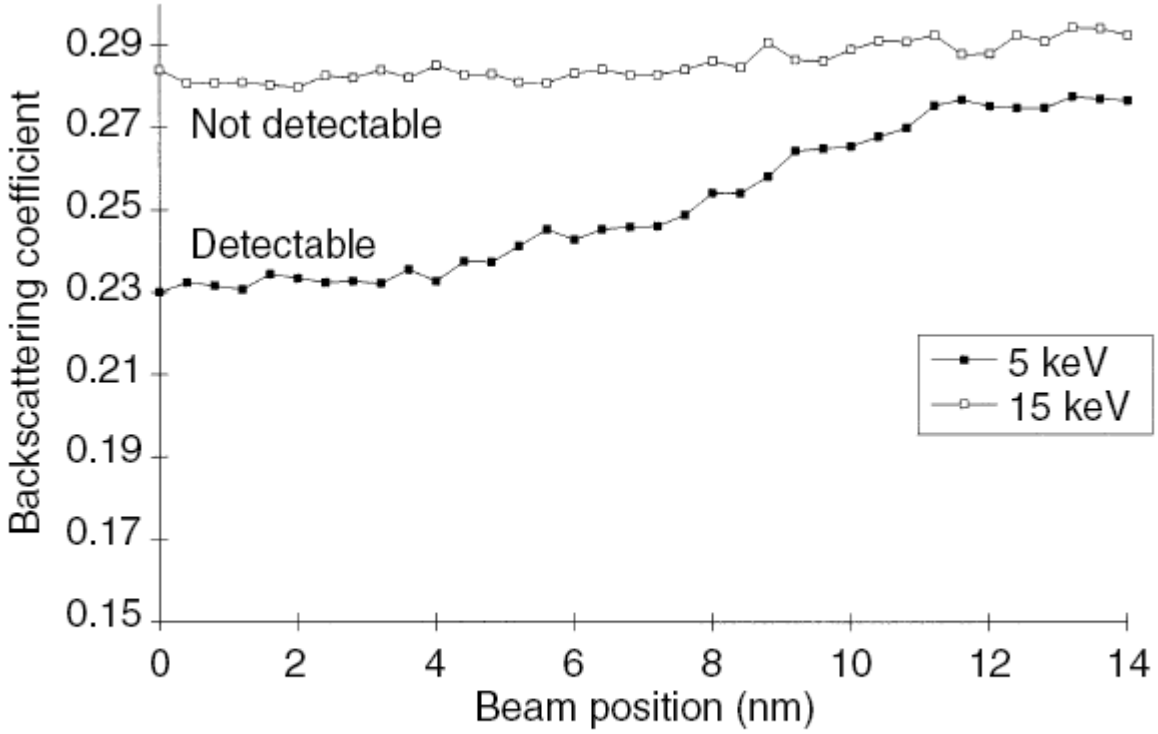

FIG. 24 Simulated profile for a 10 nm radius hemispherical inclusion of the MnS/Fe system at $E_o = 5$ and 15 keV.

R. Gauvin, P. Hovington, D.Drouin (1995) SCANNING, Vol. 17, 202–219.

Electron Probe Diameter

The relationships between the probe diameter *d* and the convergence angle *α* are

$$d = \sqrt{d_g^2 + d_s^2 + d_d^2 + d_c^2}$$

$$d_g = \sqrt{\frac{4I_p}{\pi^2 \beta \alpha^2}}$$

$$d_s = \frac{1}{2} C_s \alpha^3$$

$$d_d = \frac{0.61\lambda}{\alpha}$$

$$d_c = C_c \alpha \frac{\Delta E}{E_0}$$

Cold Field Emitter
Invented by Albert Crewe in 1968

- $E = \frac{U}{r}$
- U = 3 kV to 5 kV
- r = 100 nm
- E ≥ 10^7 V/cm

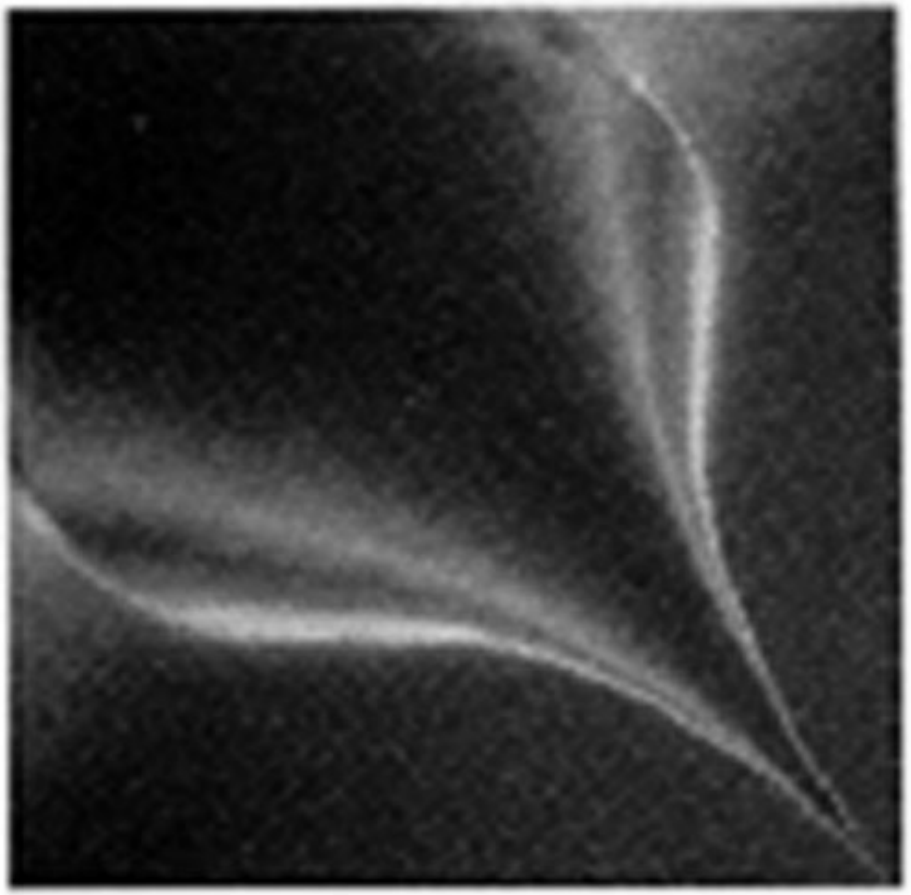

High vacuum needed (10^{-8} or 10^{-9} Pa) to avoid tip erosion

Electron Emission

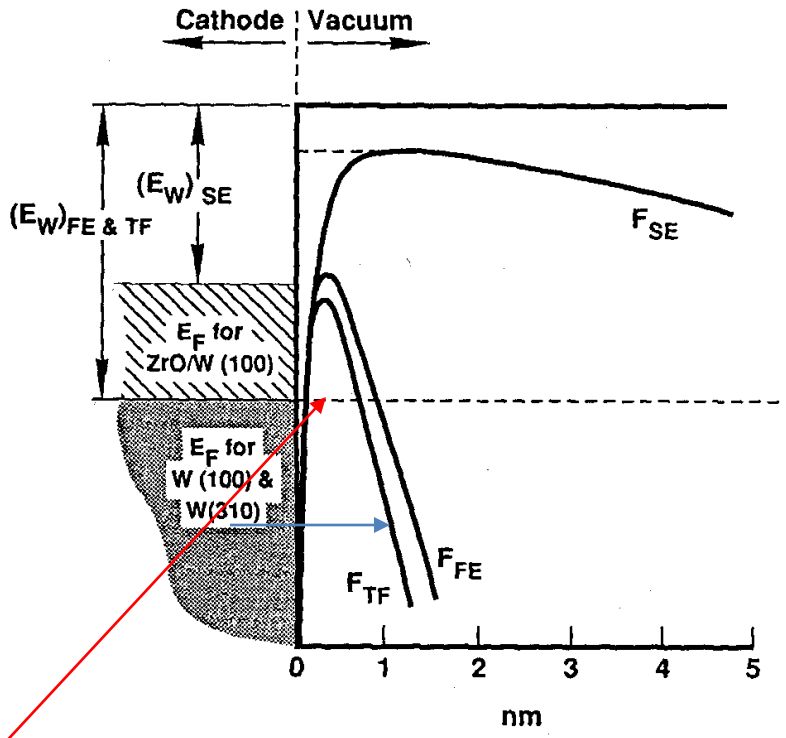

Field emission by quantum tunnel effect

True for cold field and thermal field only

Comparison of Electron Sources

Table 2.1. Comparison of Electron Sources at 20 kV

Source	Brightness (A/cm^2 sr)	Lifetime (h)	Source size	Energy spread ΔE (eV)	Beam current stability (%/h)	Ref.
Tungsten hairpin	10^5	40–100	30–100 μm	1–3	1	*a,b*
LaB_6	10^6	200–1000	5–50 μm	1–2	1	*b,c*
Field emission						
Cold	10^9	>1000	<5 nm	0.3	5	*d,e*
Thermal	10^8	>1000	<5 nm	1	5	*e*
Schottky	10^8	>1000	15–30 nm	0.3–1.0	~1	*e*

Effect of Accelerating Voltage

30 kV

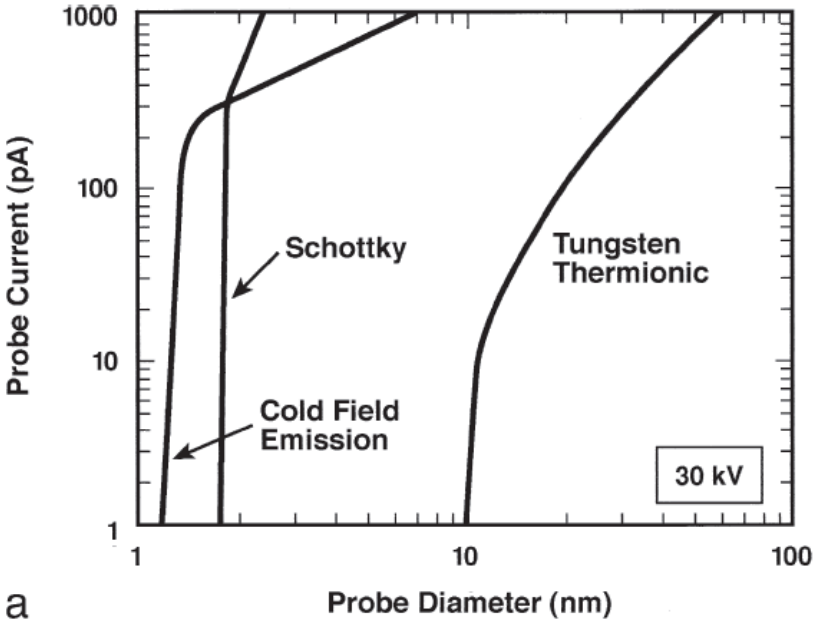

a

1 kV

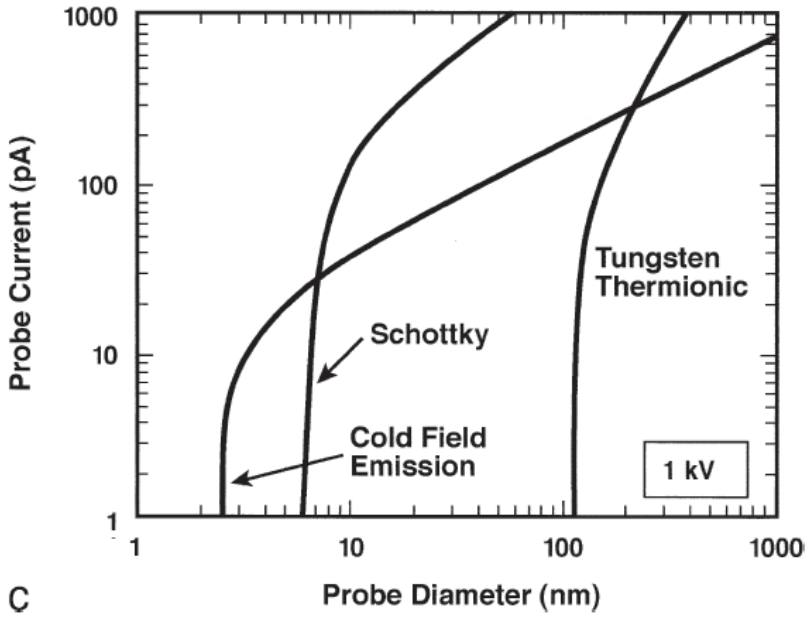

c

Cold Field Scanning Electron Microscopes, Gauvin's Group

Hitachi SU-8000 (2010)

0.5 nm at 30 keV
2 nm at 0.2 keV

Hitachi SU-8230 (2014)

0.4 nm at 30 keV,
1.8 nm at 0.2 keV

SU-8230, Auto Flash

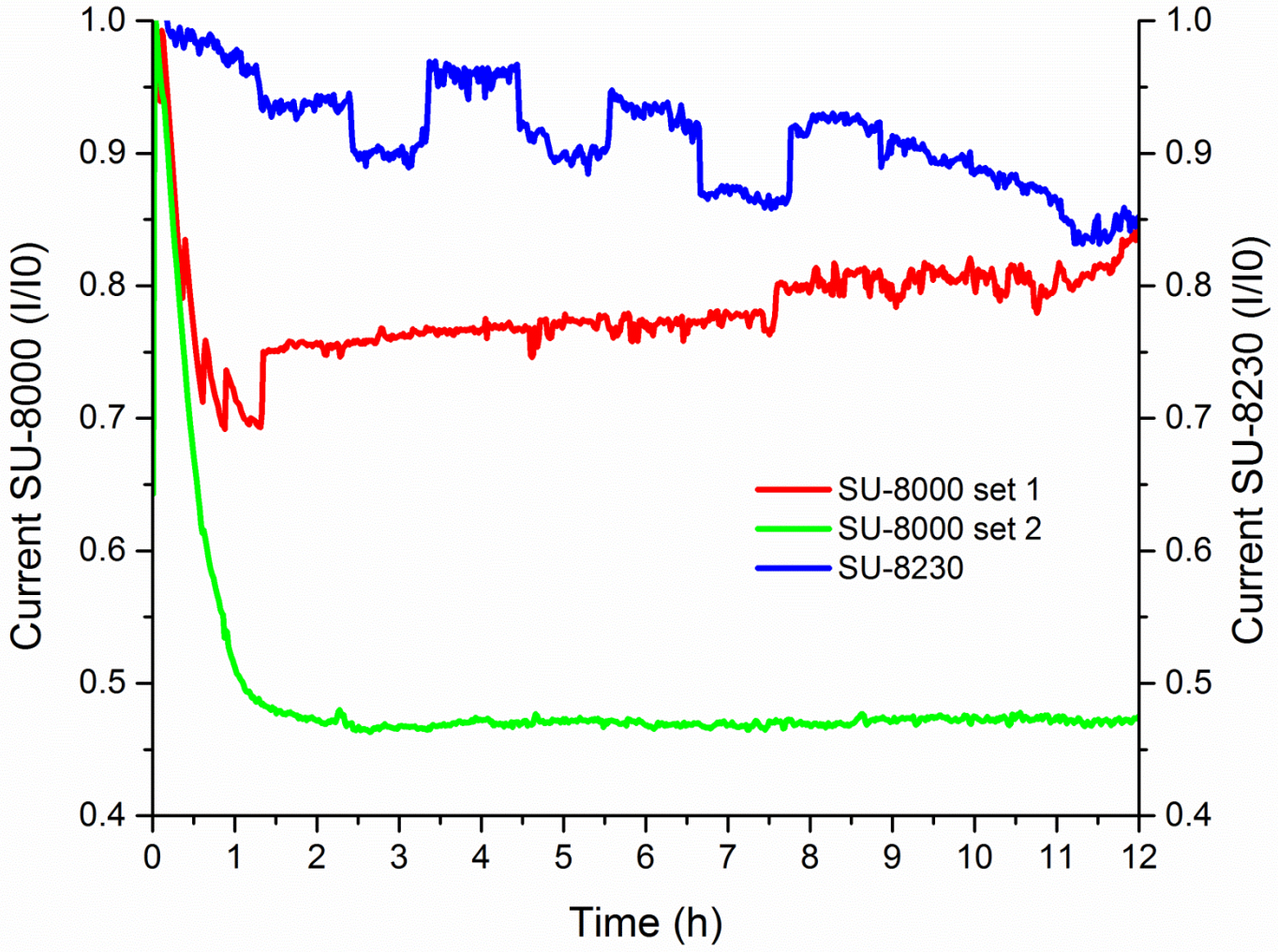

HITACHI SU-8XXX Series

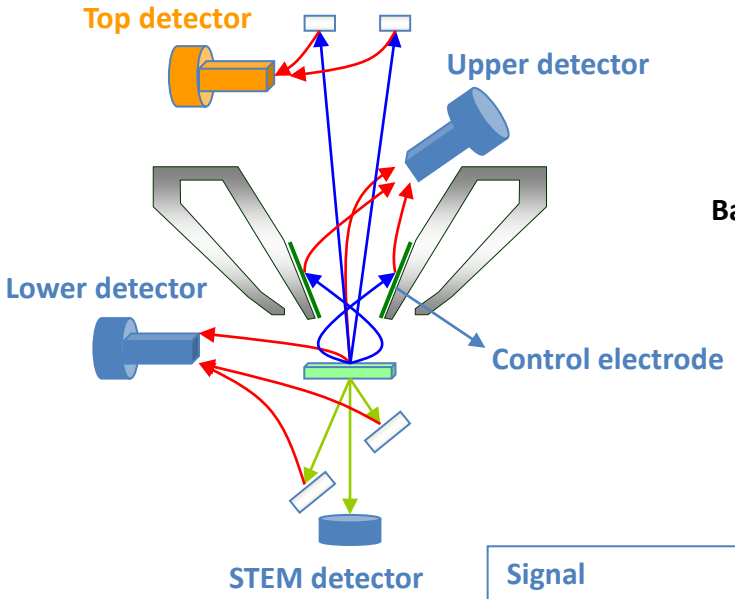

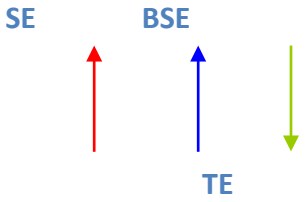

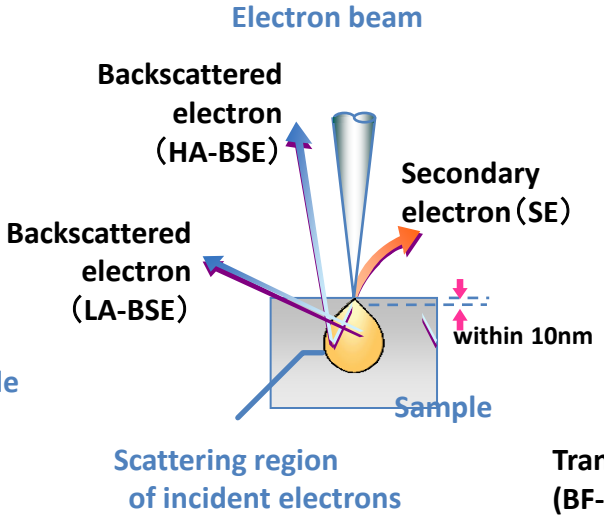

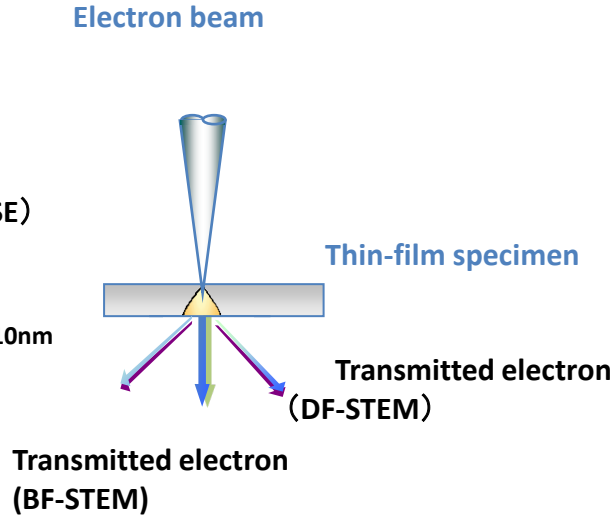

Signal	Abbrev.	Detector	Included information
Backscattered electron	HA-BSE	Top	Compositional + Crystal
Backscattered electron	LA-BSE	Upper	Compositional + Crystal +Topographical (with Charge reduction)
Secondary electron	SE	Upper	surface (incl. Voltage contrast)
Secondary electron	Lower	Lower	Topographical
Transmitted electron	BF-STEM	STEM	Internal + Crystallographic
Transmitted electron	DF-STEM	Lower	Internal + Compositional

Al – Li alloy, 2199

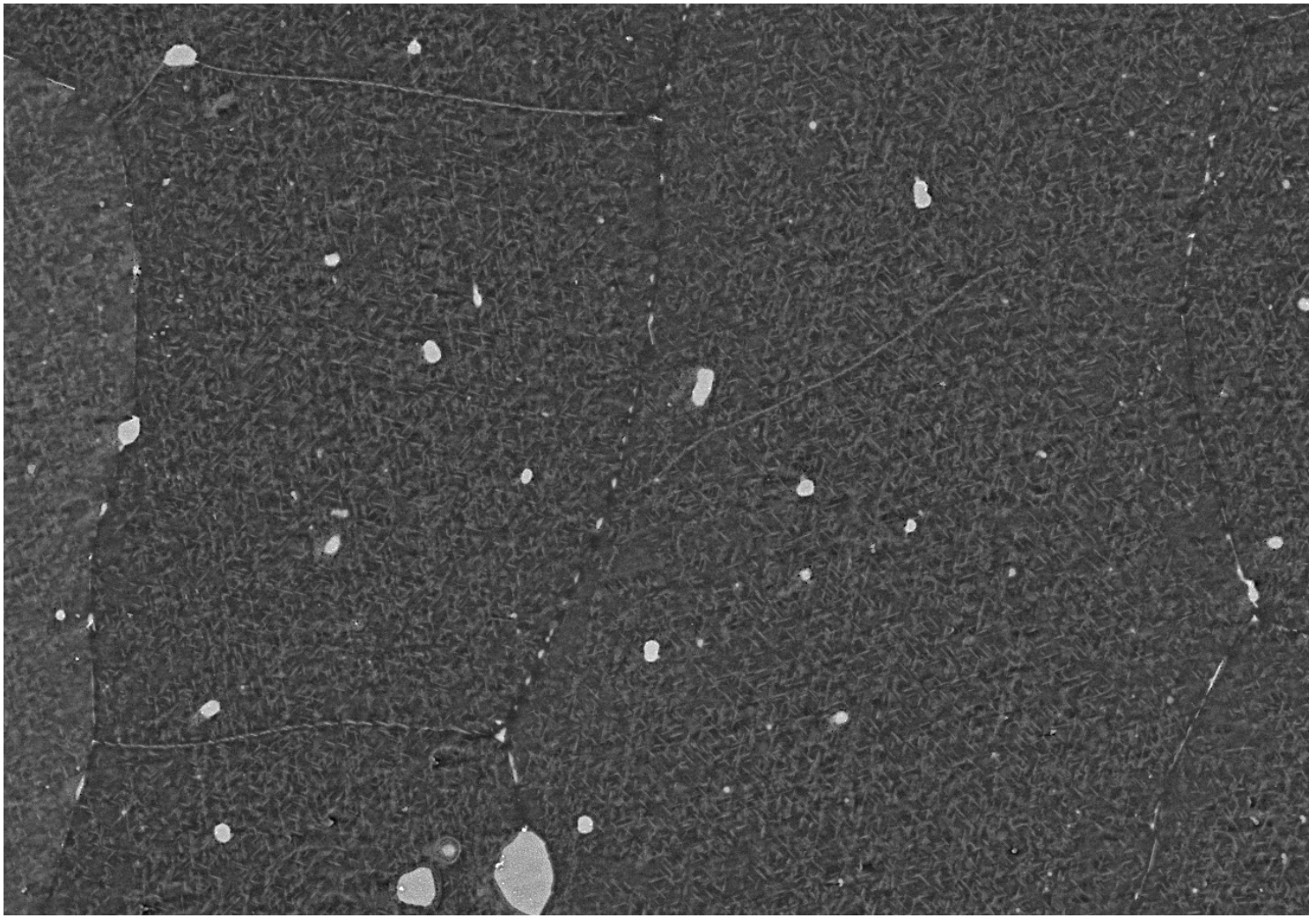

Al - Li Alloy 2099

LA100(U)

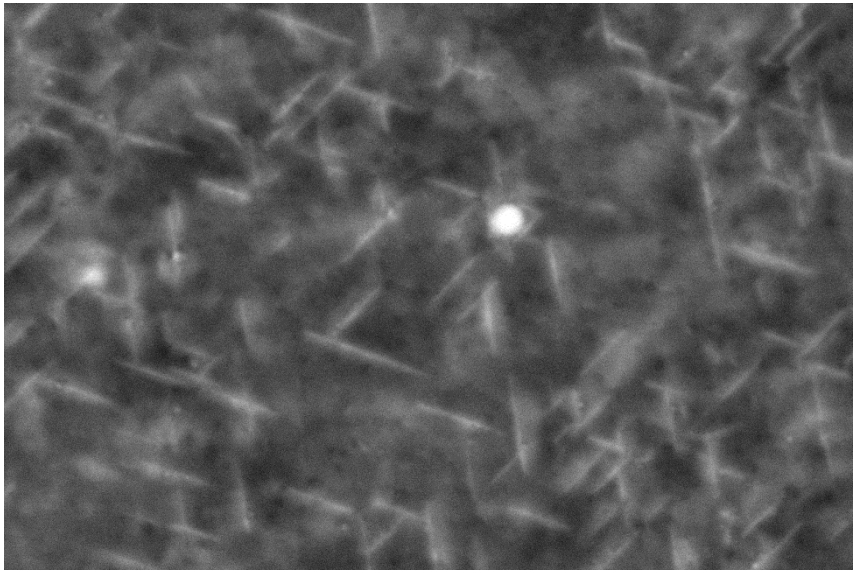

FOV 1270 nm
100 kX
SNR: 1.5
Resolution: 10.0 nm

LA100(U)

δ′ (Al_3Li)

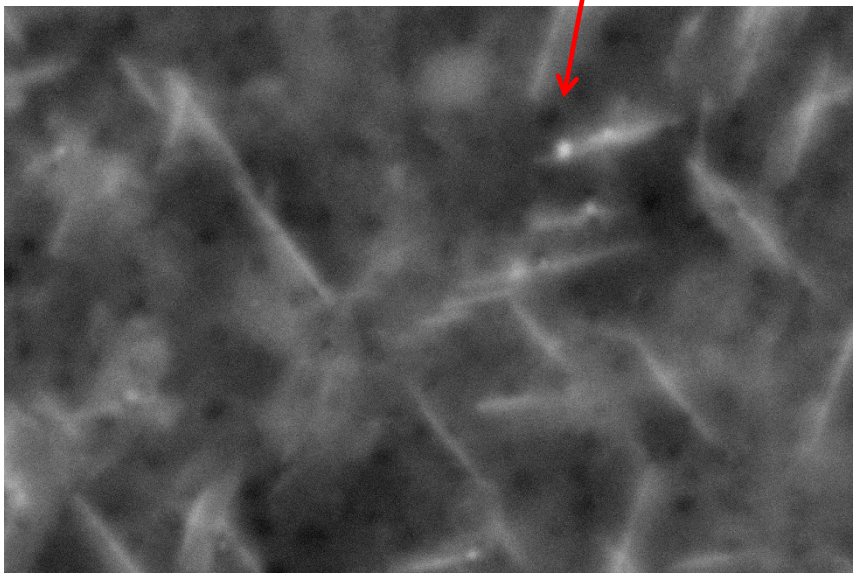

FOV: 635 nm
200 kX
SNR: 1.6
Resolution: 6.6 nm

Nonconductive Materials

- At E_2 and E_1, no charging.
- Ceramics, $E_2 \approx 3 - 4$ keV.
- Polymers, $E_2 \approx 0.5$ keV.

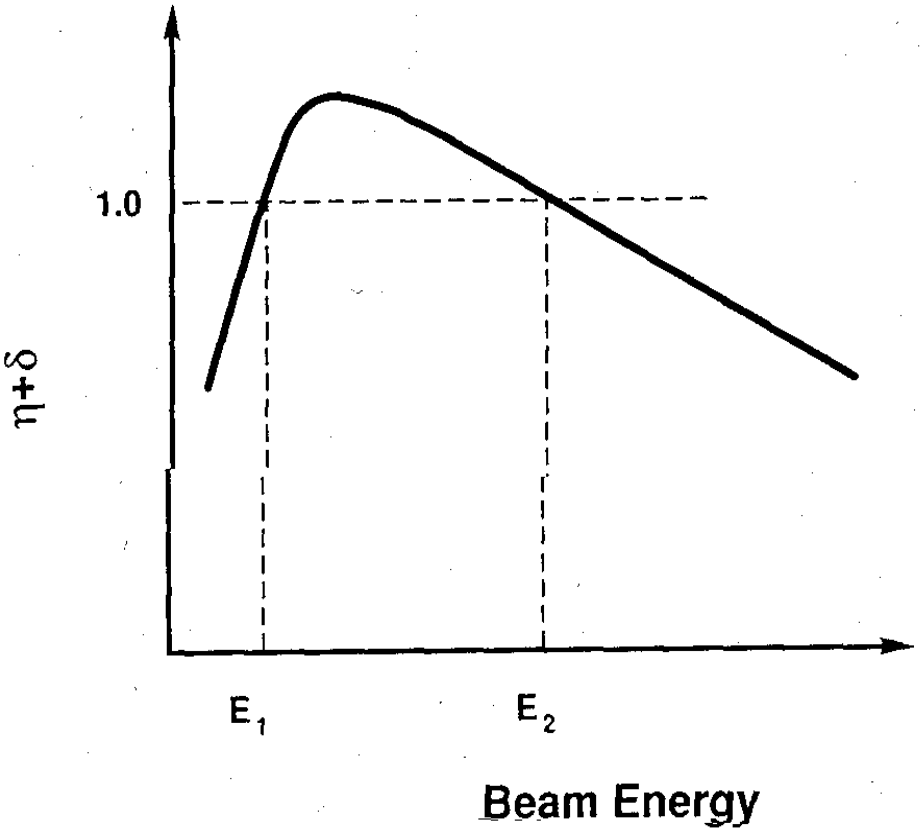

Alumina, 0.7 keV

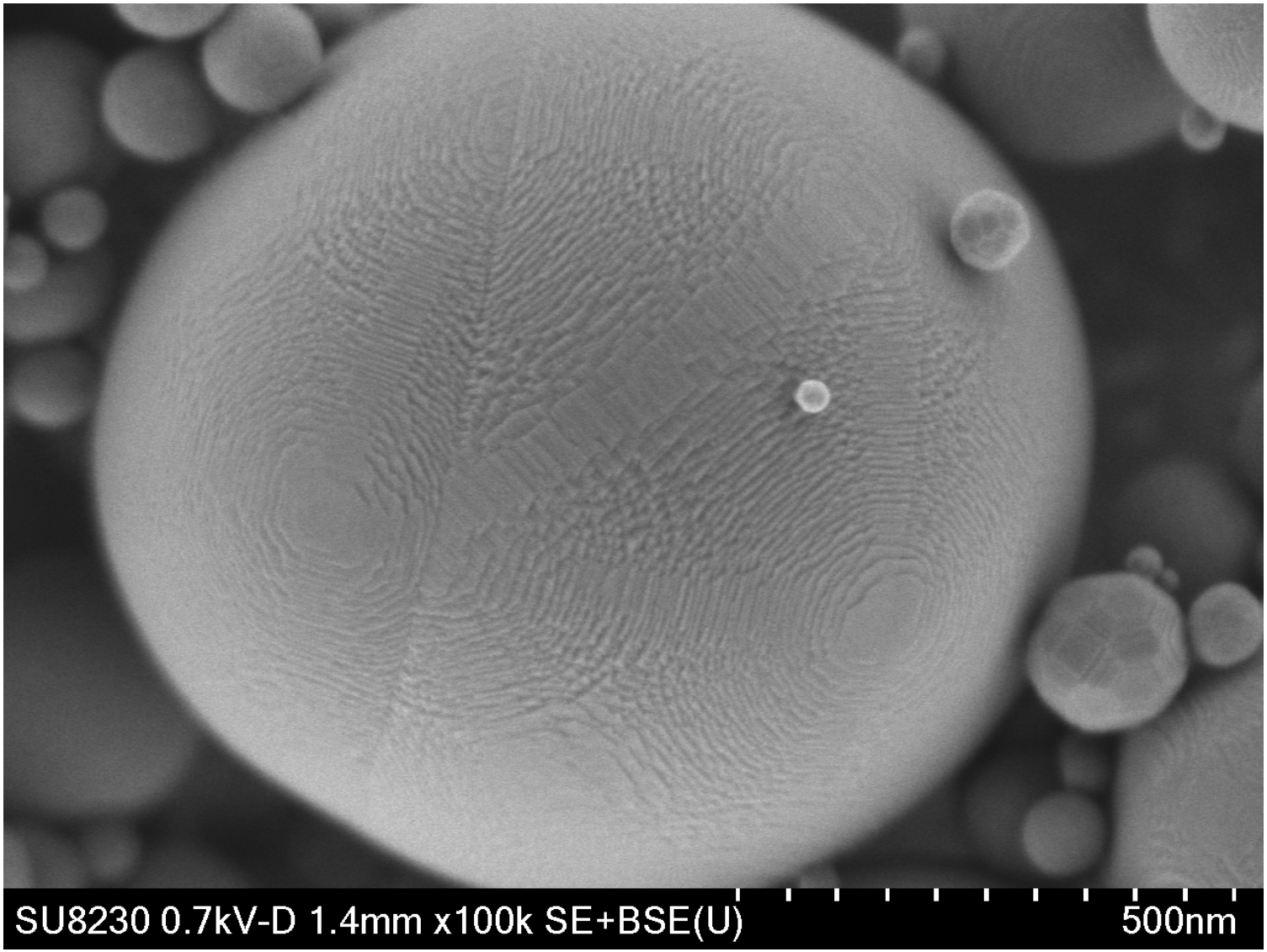

Low Accelerating Voltage and Charging effect: Alumina spheres

Upper

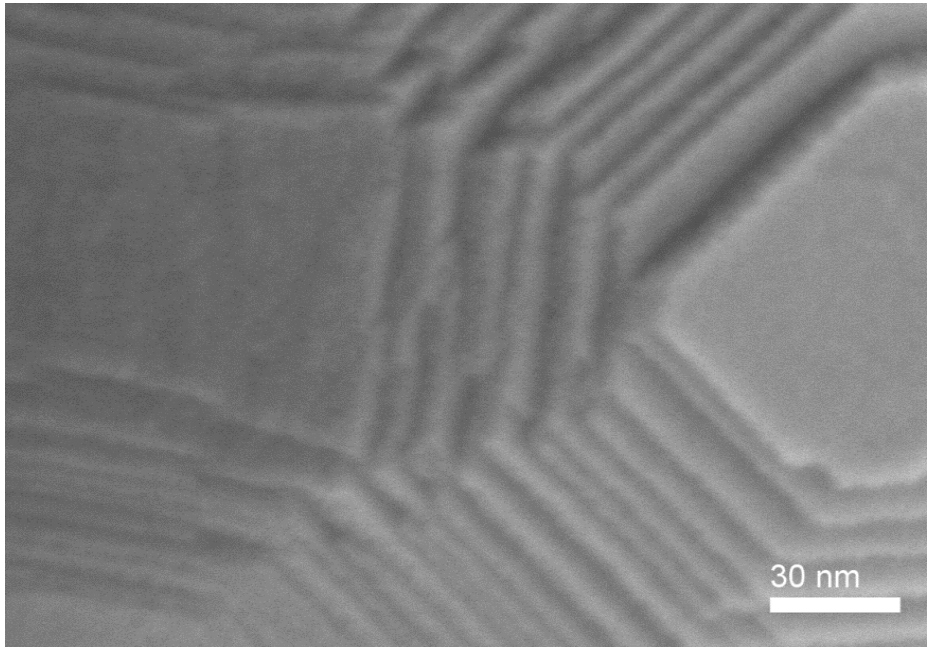

TOP

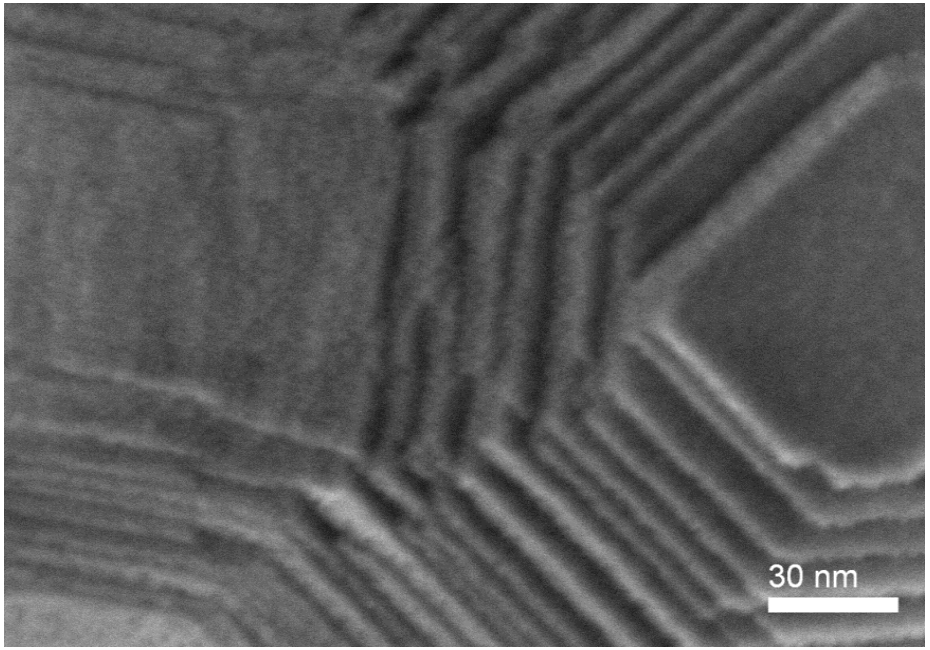

Effect of Auto-Flash Alumina Powder

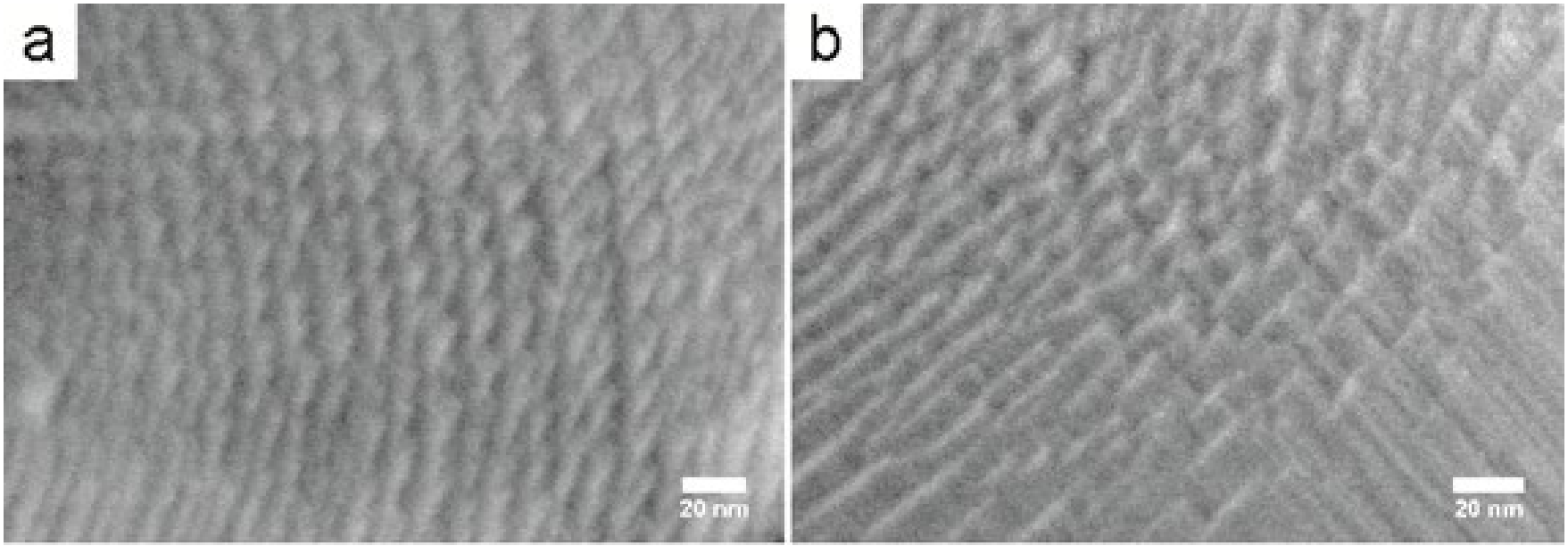

SU-8000 **SU-8230**

MgO ash on Al substrate

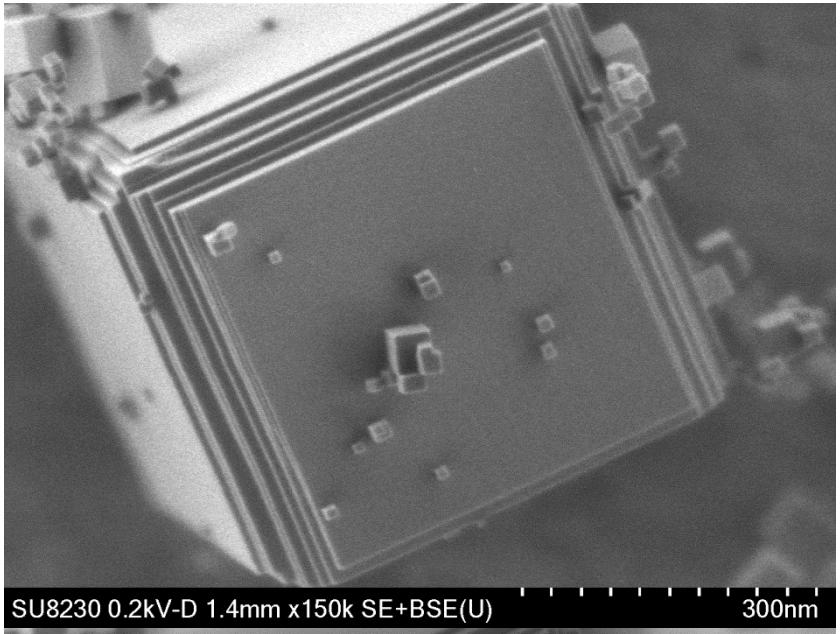

Upper detector

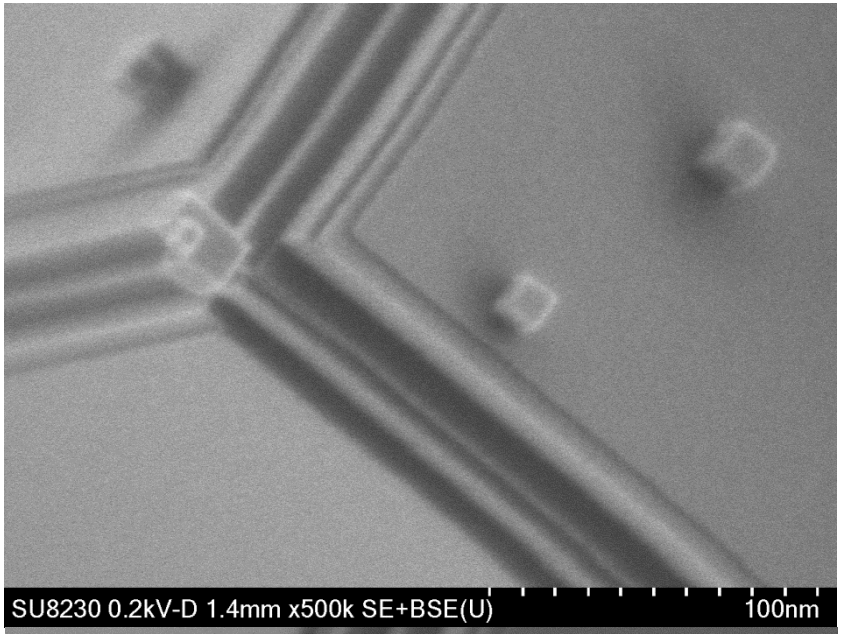

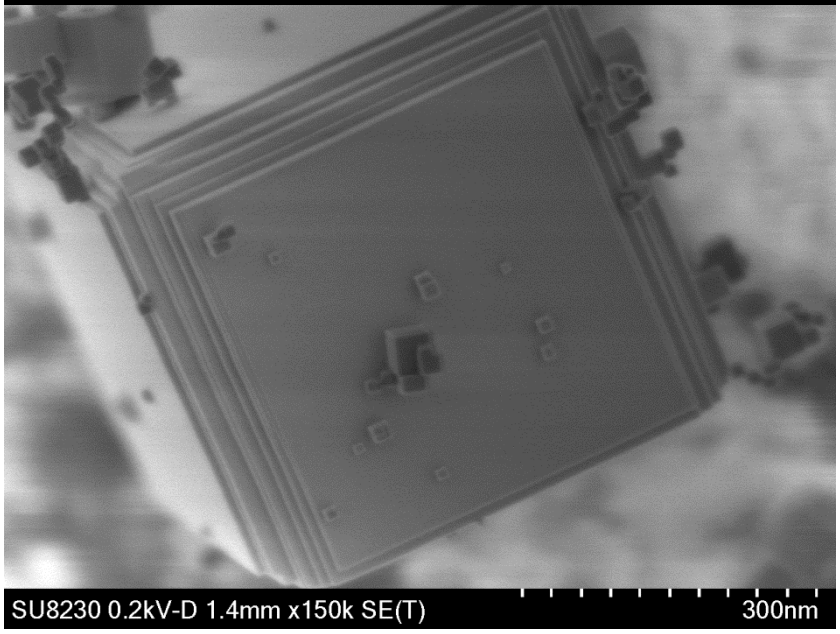

Top detector

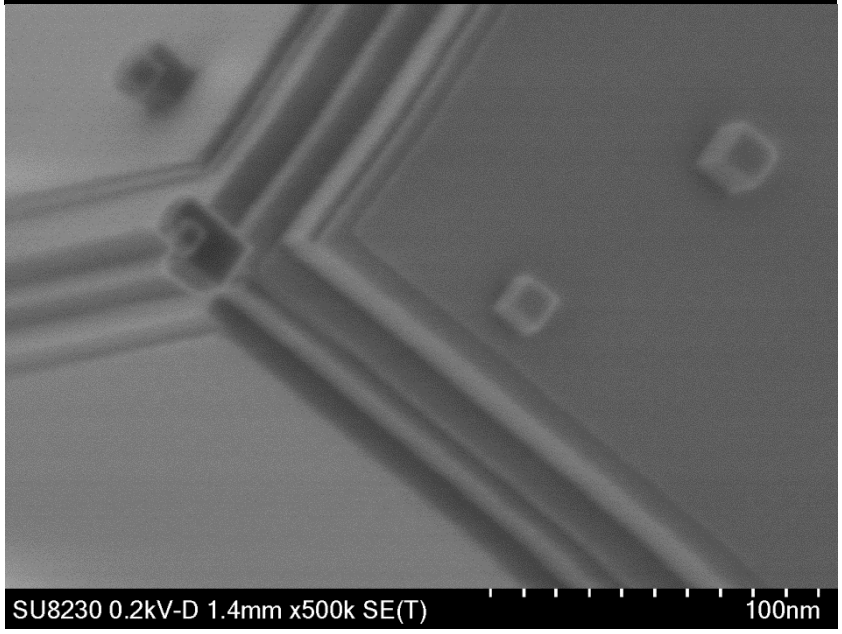

X-Max

400000 cps @ 80 mm2

In practice

Detector area	20mm²	50mm²	80mm²
Resolution (eV):			
MnK_{α} resolution	129	129	129
Operating angle	0° to 45°		
Temperature range	10°C to 30°C		
Altitude	Sea level to 1,500m		

40 nm Al_3Zr Precipitate, 3 kV, Al 2099

Experiment

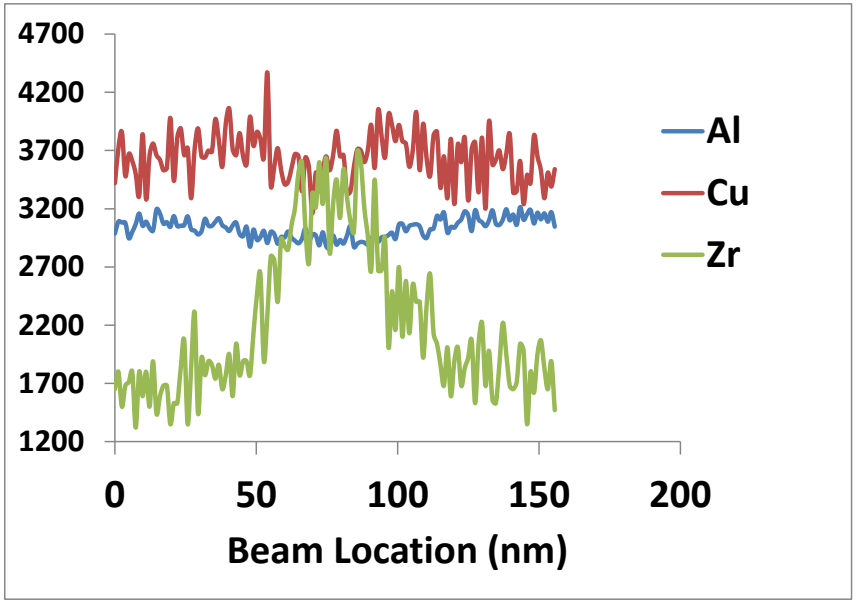

Monte Carlo MC X-Ray

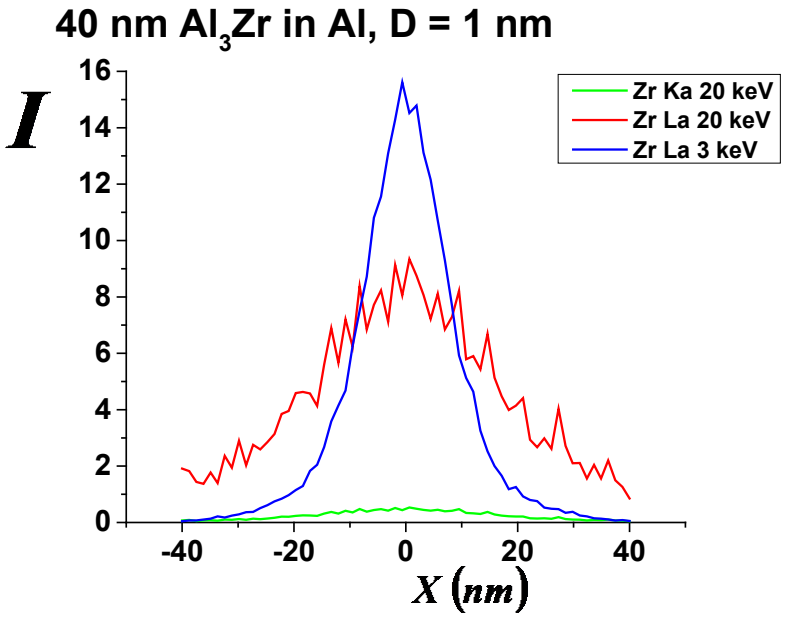

Mg – Al – Ca alloy
3 keV EDS, SU 8000, Oxford XMax 80

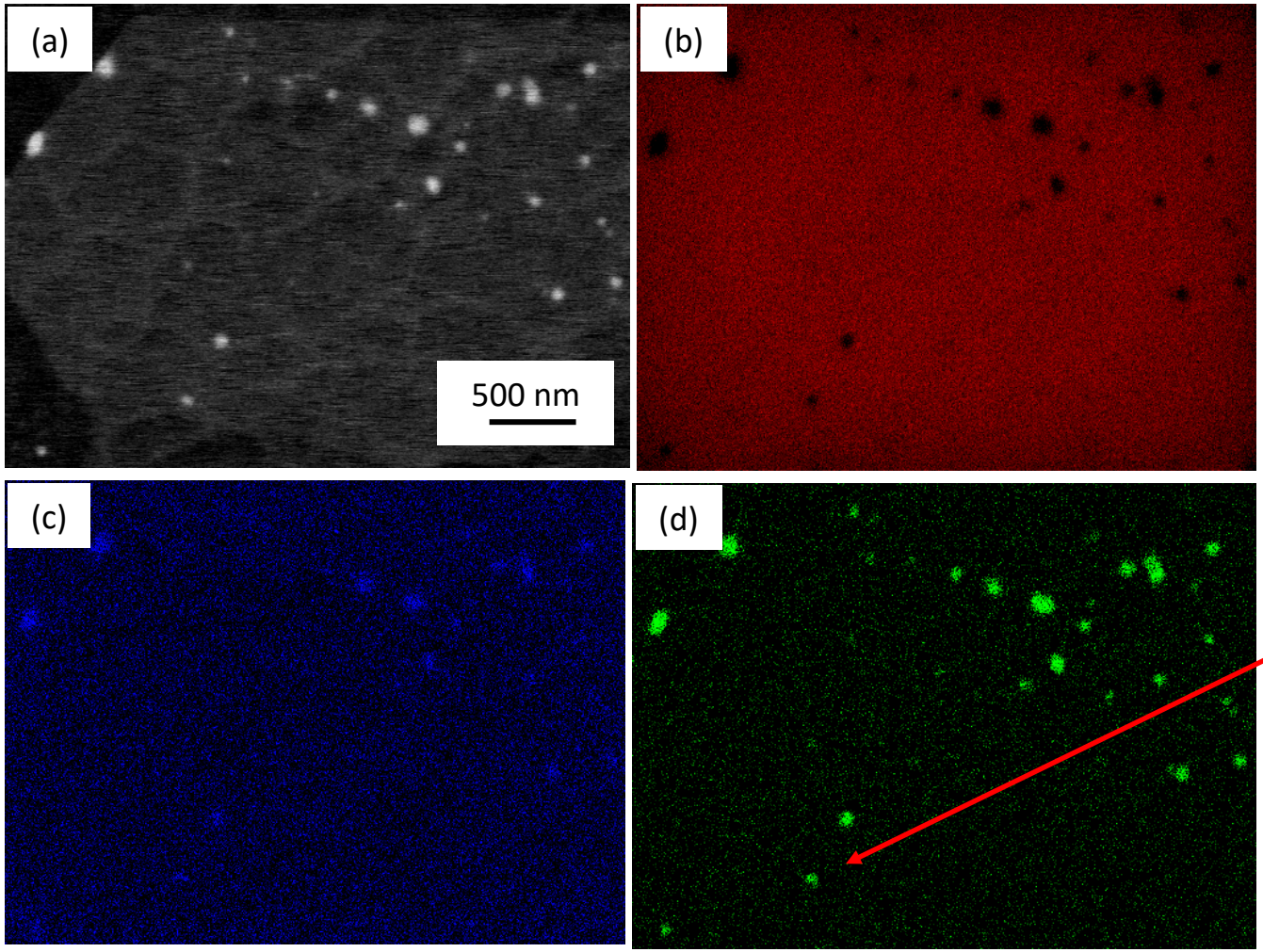

Figure 7. (a) SEM-BSE image, (b) Mg, (c) Al and (Ca) X-ray maps

Quantitative X-Ray Microanalysis
The f Ratio Method

$$f_A = \frac{I_A}{I_A + I_B}$$

P. Horny, E. Lifshin, H. Campbell and R. Gauvin (2010), “Development of a New Quantitative X-Ray Microanalysis Method for Electron Microscopy”, Microscopy & Microanalysis, Vol. 16, No. 6, pp. 821-830.

Grain Boundary Diffusion

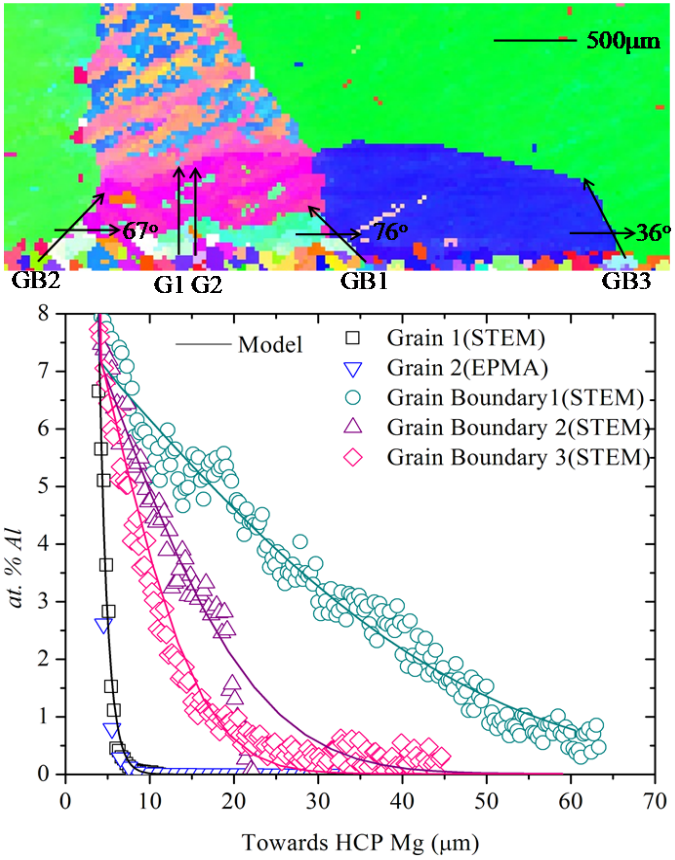

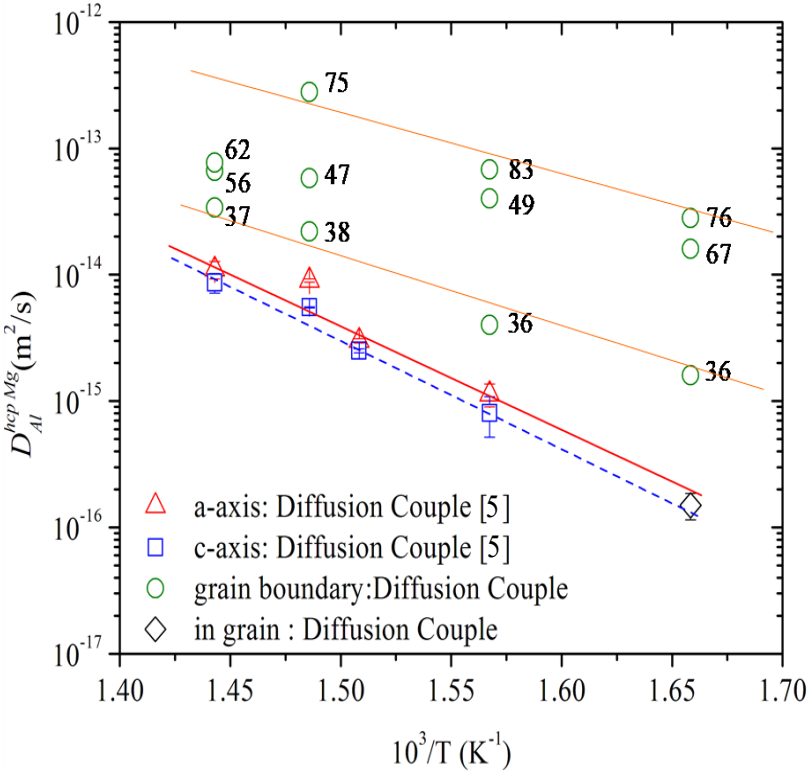

S. K. Das, N. Brodusch, R. Gauvin and I.-H. Jung (2014), "Grain boundary diffusion of Al in Mg", Scripta Materialia, 80, pp. 41-44.

Electron Channelling

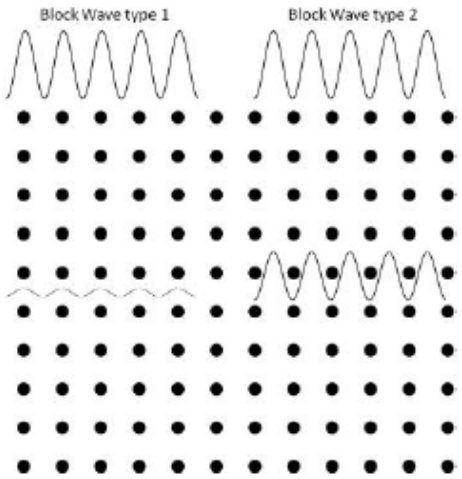

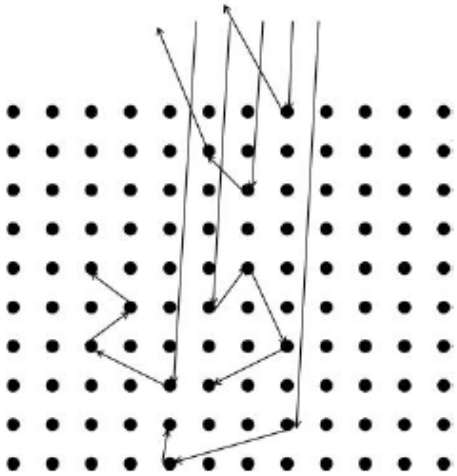

Low retrodiffusion yield

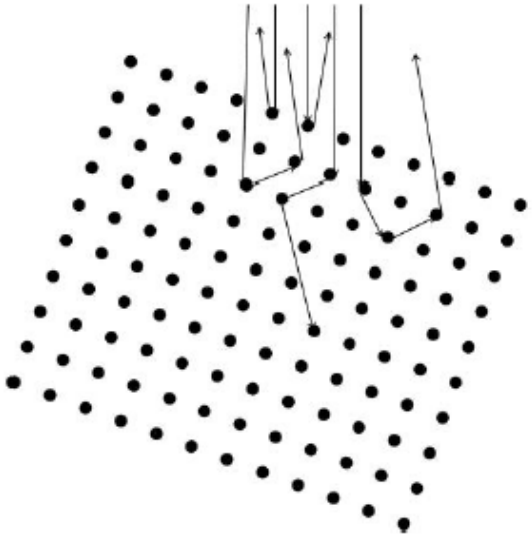

High retrodiffusion yield

!!!Dislocations in SEM!!!

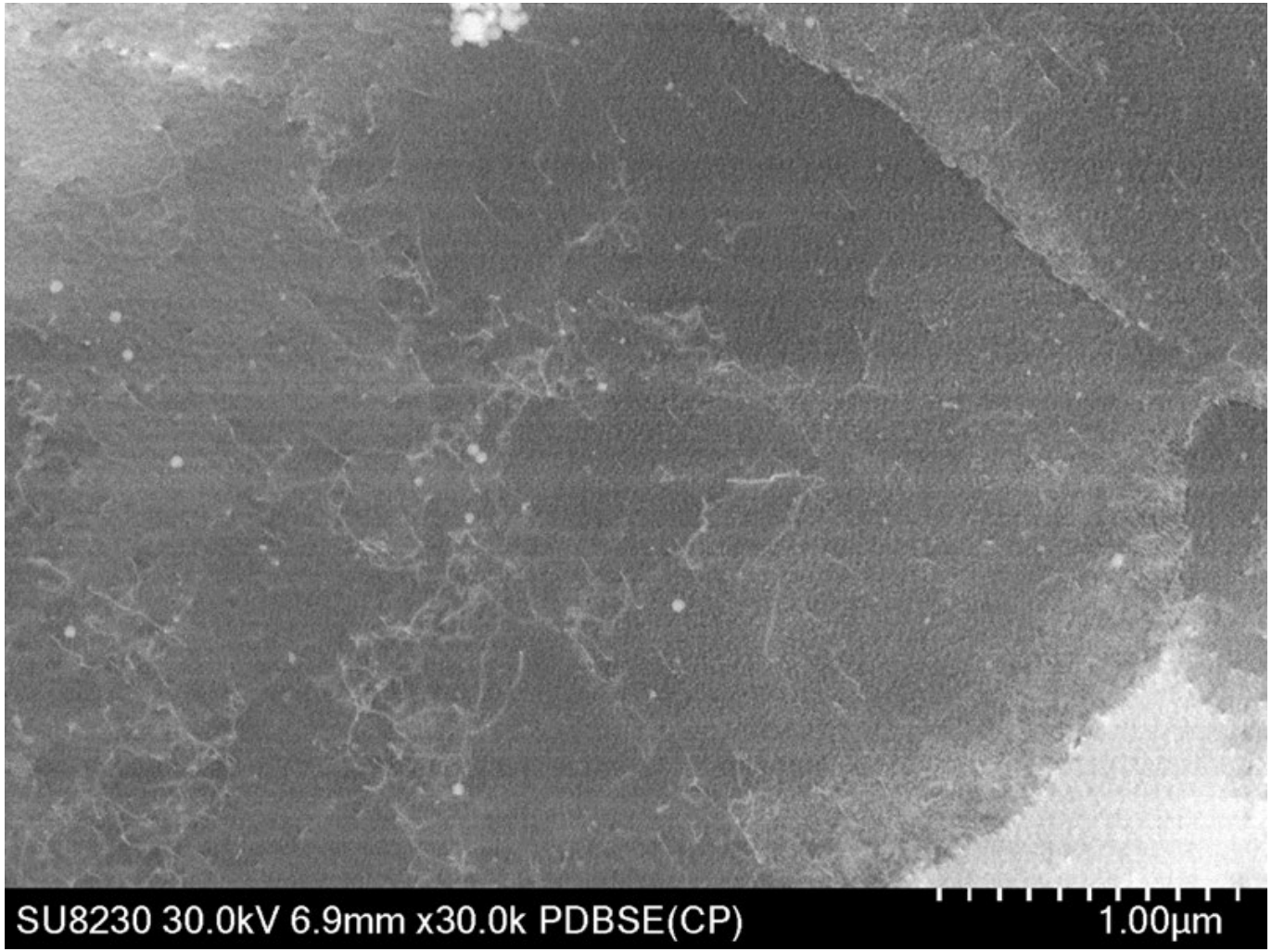

STEM, Al, 30 kV, 80 nm

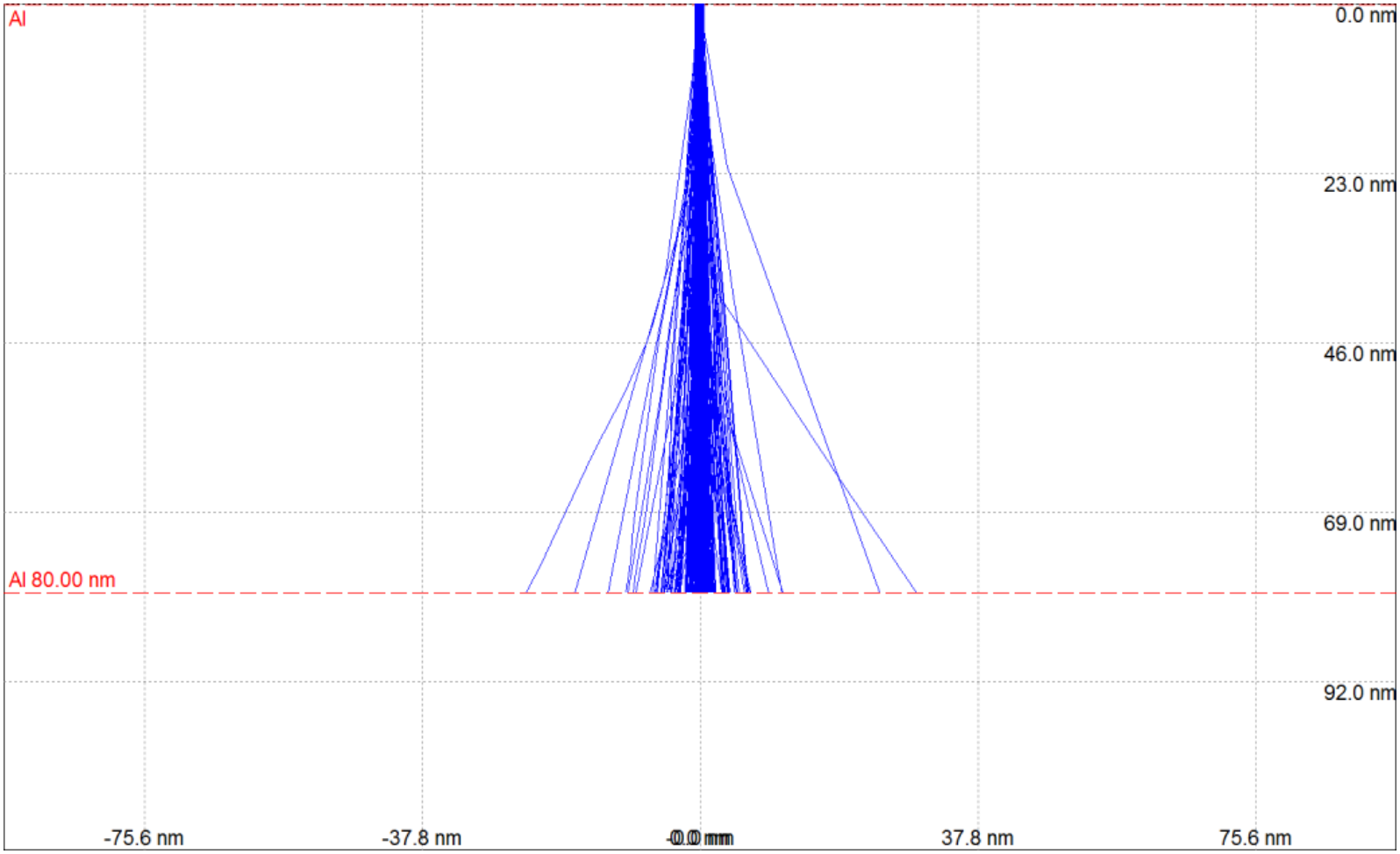

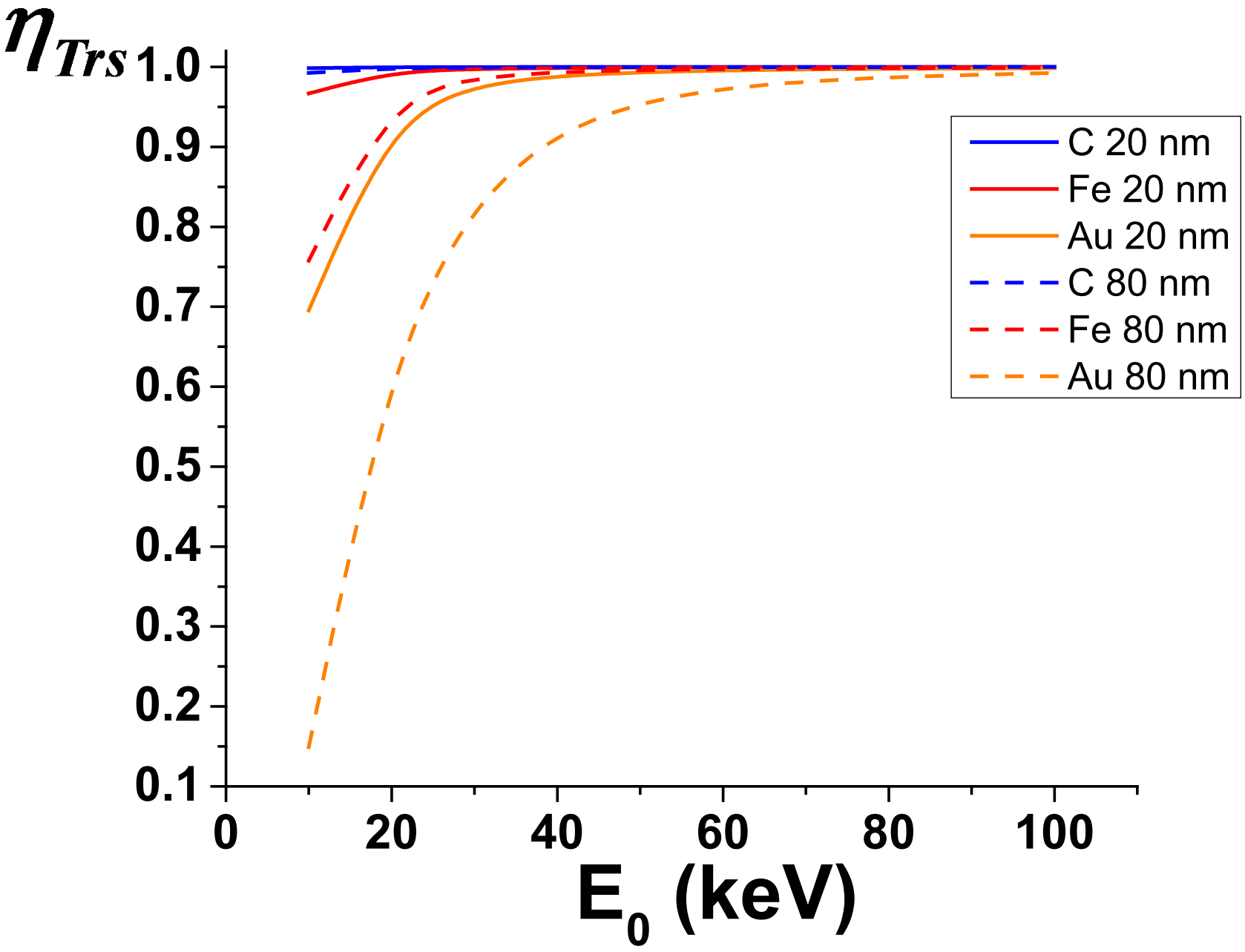
η_{Trs}
1.0
0.9
0.8
0.7
0.6
0.5
0.4
0.3
0.2
0.1
0
20
40
60
80
100
E_0 (keV)
C 20 nm
Fe 20 nm
Au 20 nm
C 80 nm
Fe 80 nm
Au 80 nm

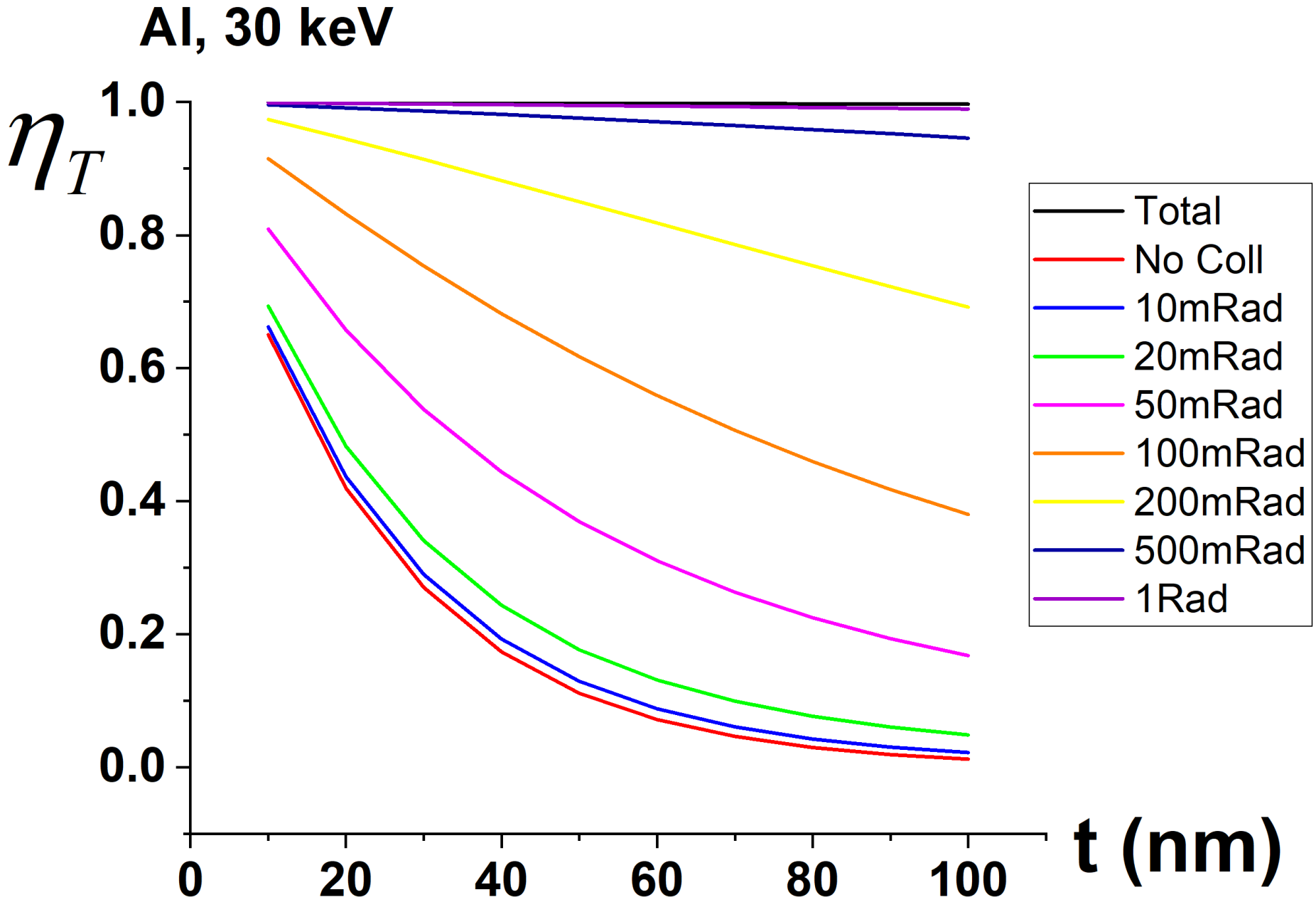
Al, 30 keV
η_T
1.0
0.8
0.6
0.4
0.2
0.0
0
20
40
60
80
100
t (nm)
Total
No Coll
10mRad
20mRad
50mRad
100mRad
200mRad
500mRad
1Rad

Al –Mg Chips

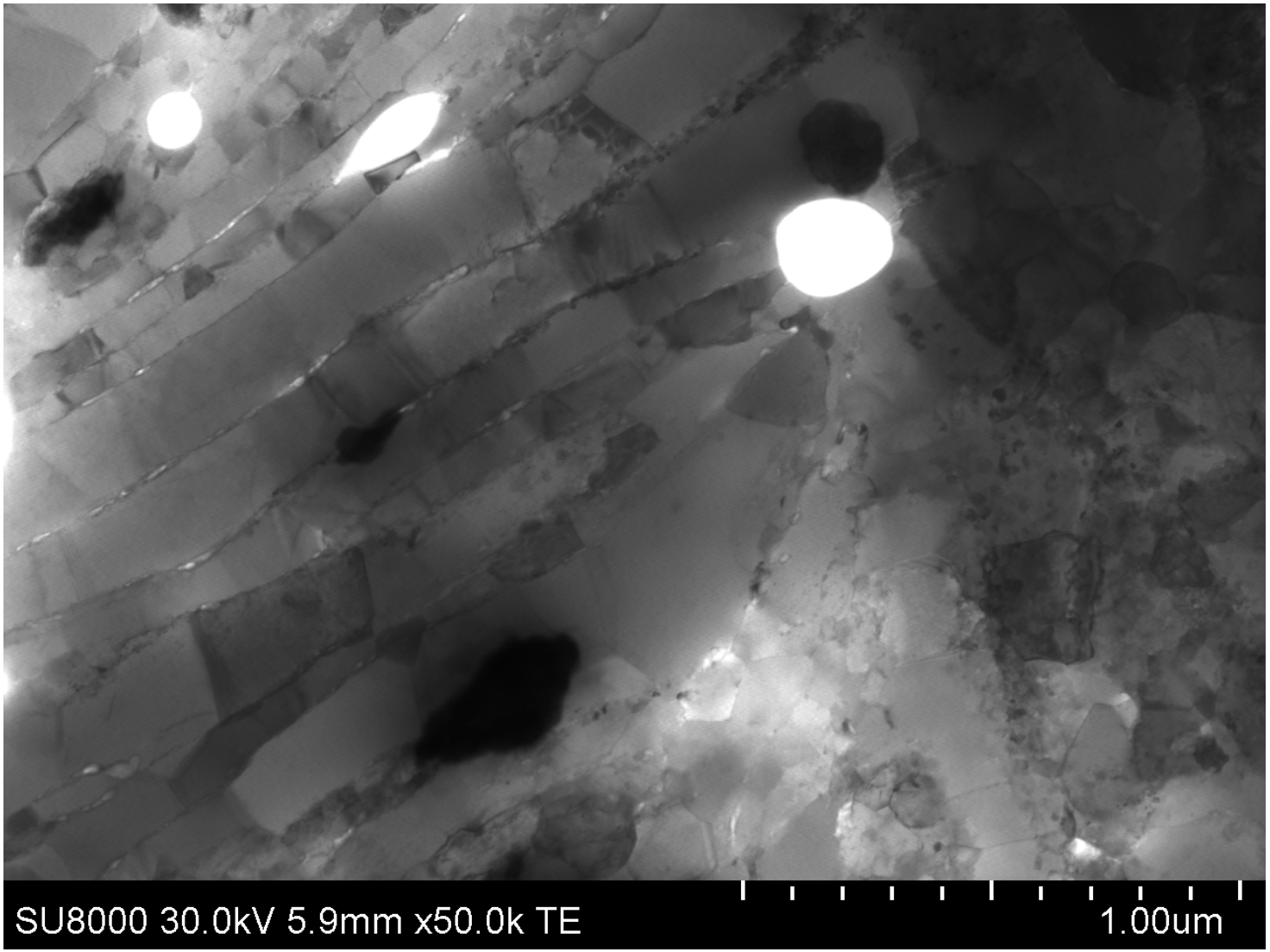

Reciprocity STEM - CTEM

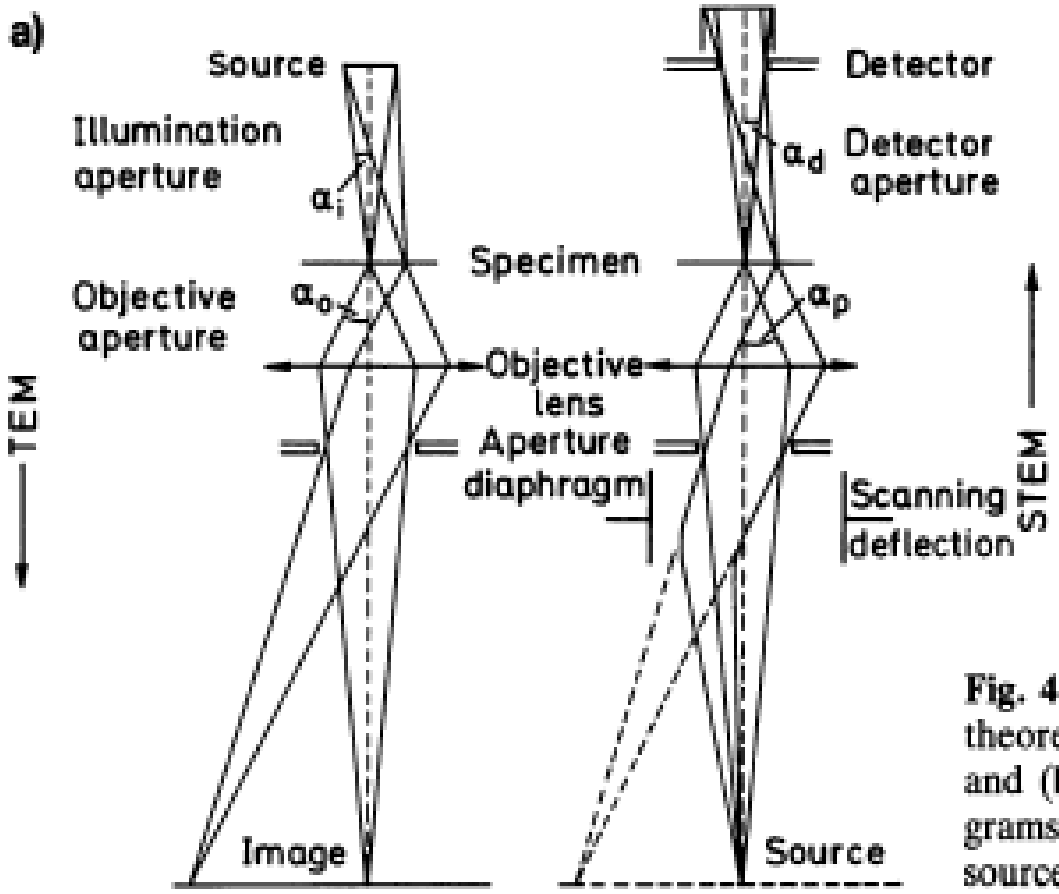

$$\alpha_i = \alpha_d$$

Fig. 4.26 a, b. Demonstration of the theorem of reciprocity for (a) TEM and (b) STEM in terms of ray diagrams connecting the intermediate source and image

From Reimer (1984)

Aperture 3 (β = 3.3 mrad)

WD = 15 mm

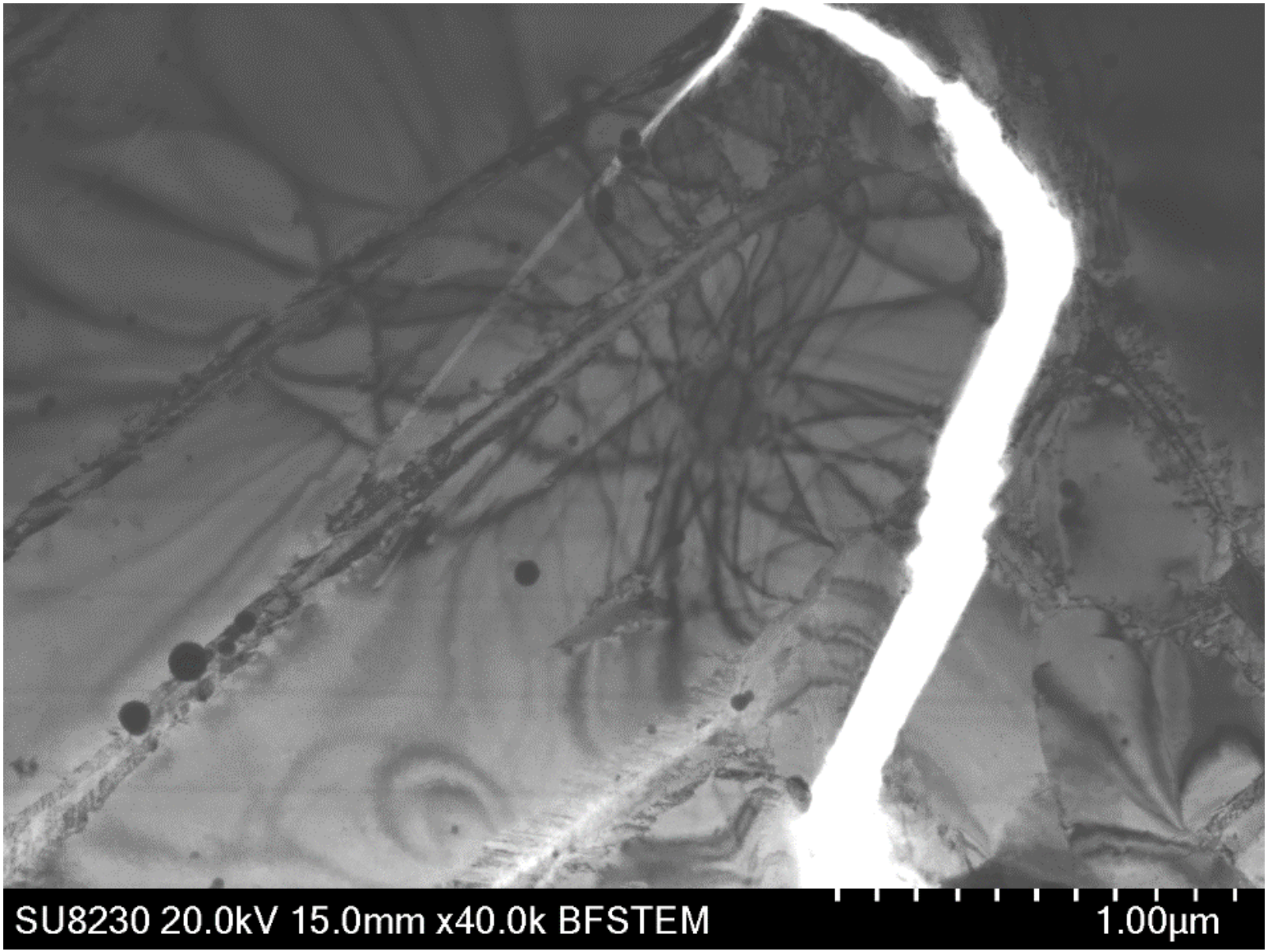

CNT covered with Pt/Ni nanoparticles
E0 = 10 kV

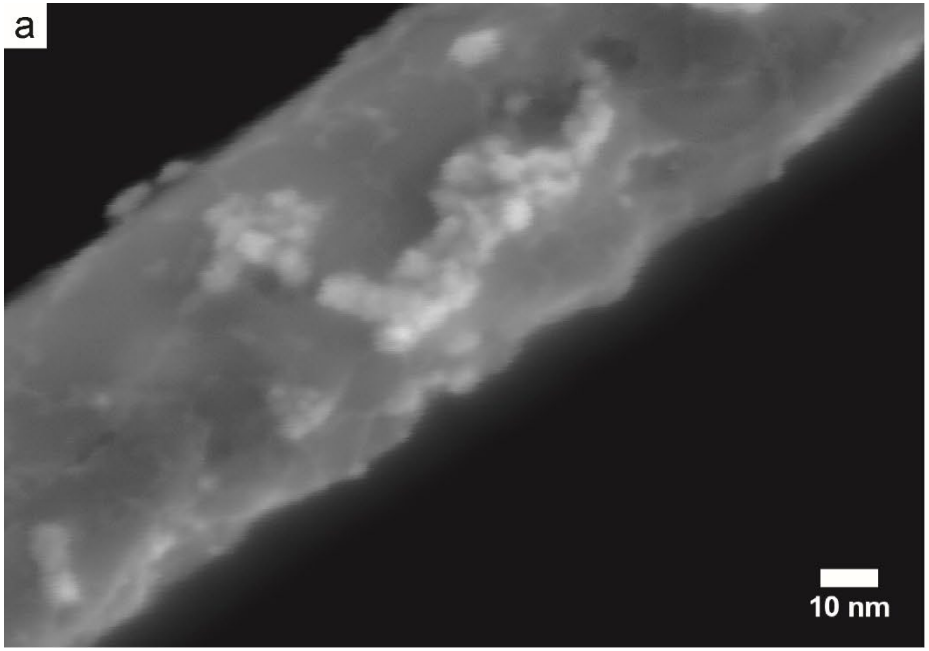

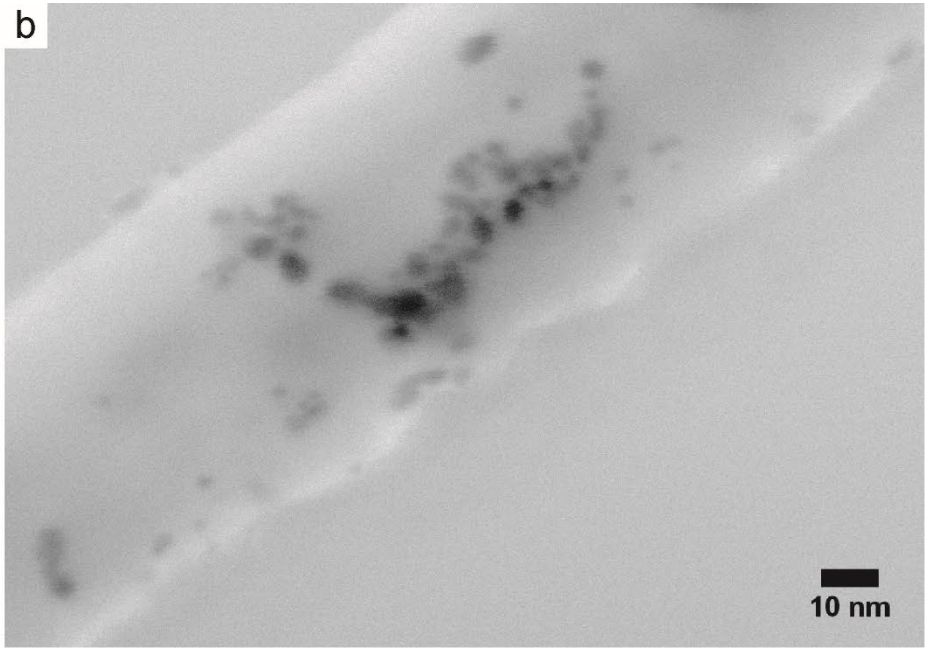

SE

BF

Al 2099, 30 keV, BF

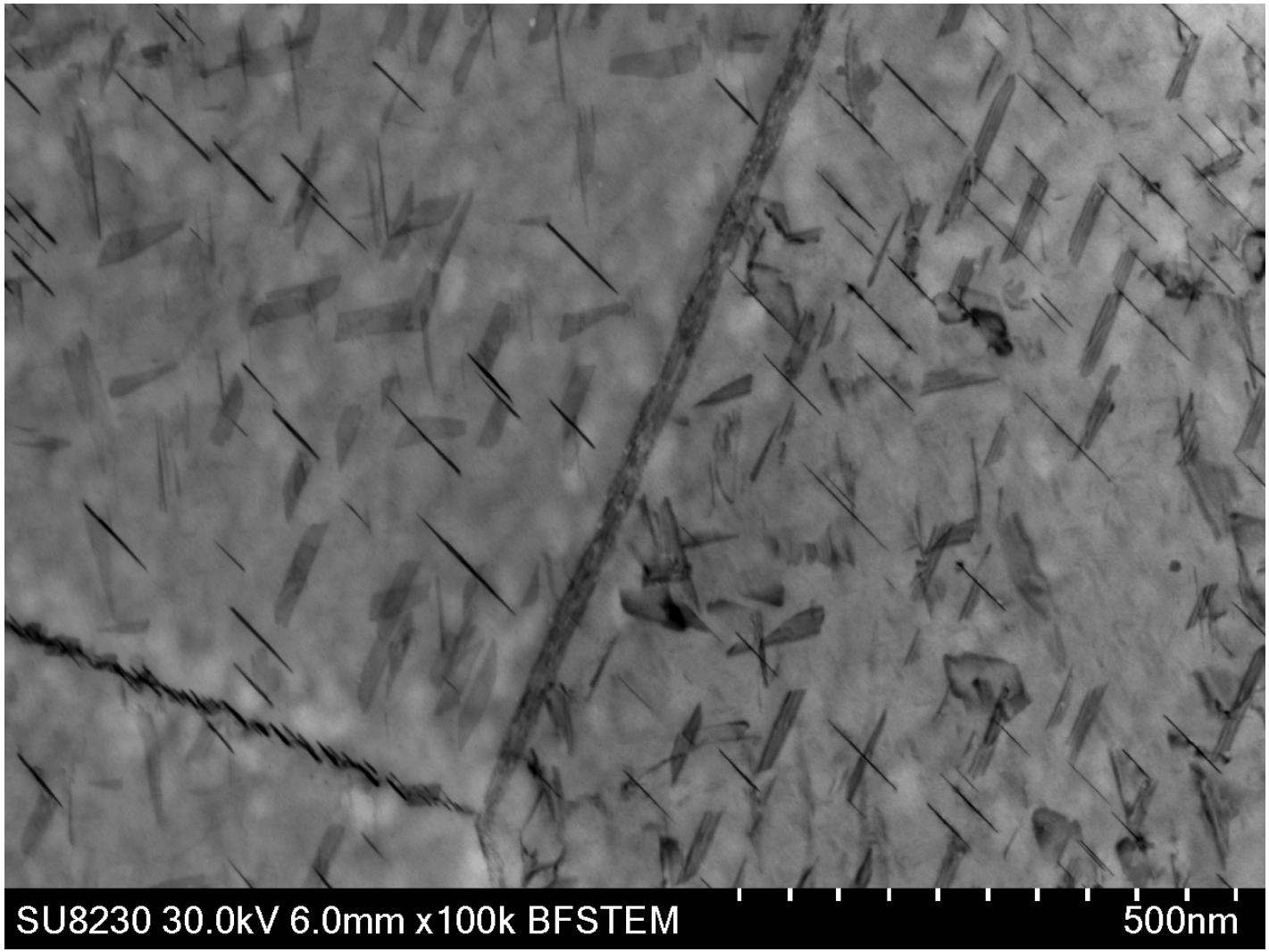

Al 2099, 30 keV, DF

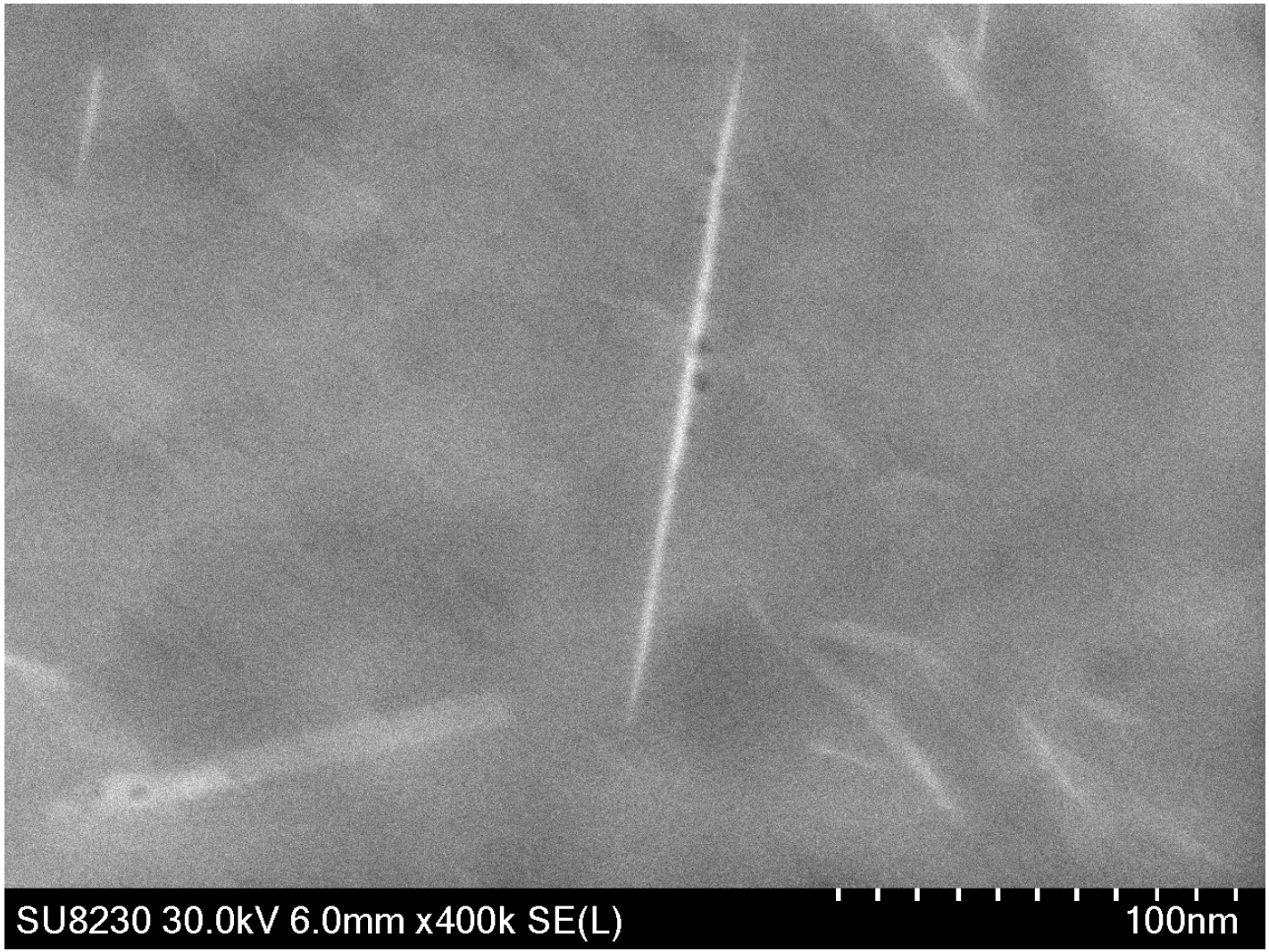

δ’ (Al_3Li) in 80 nm Al, 11 M e

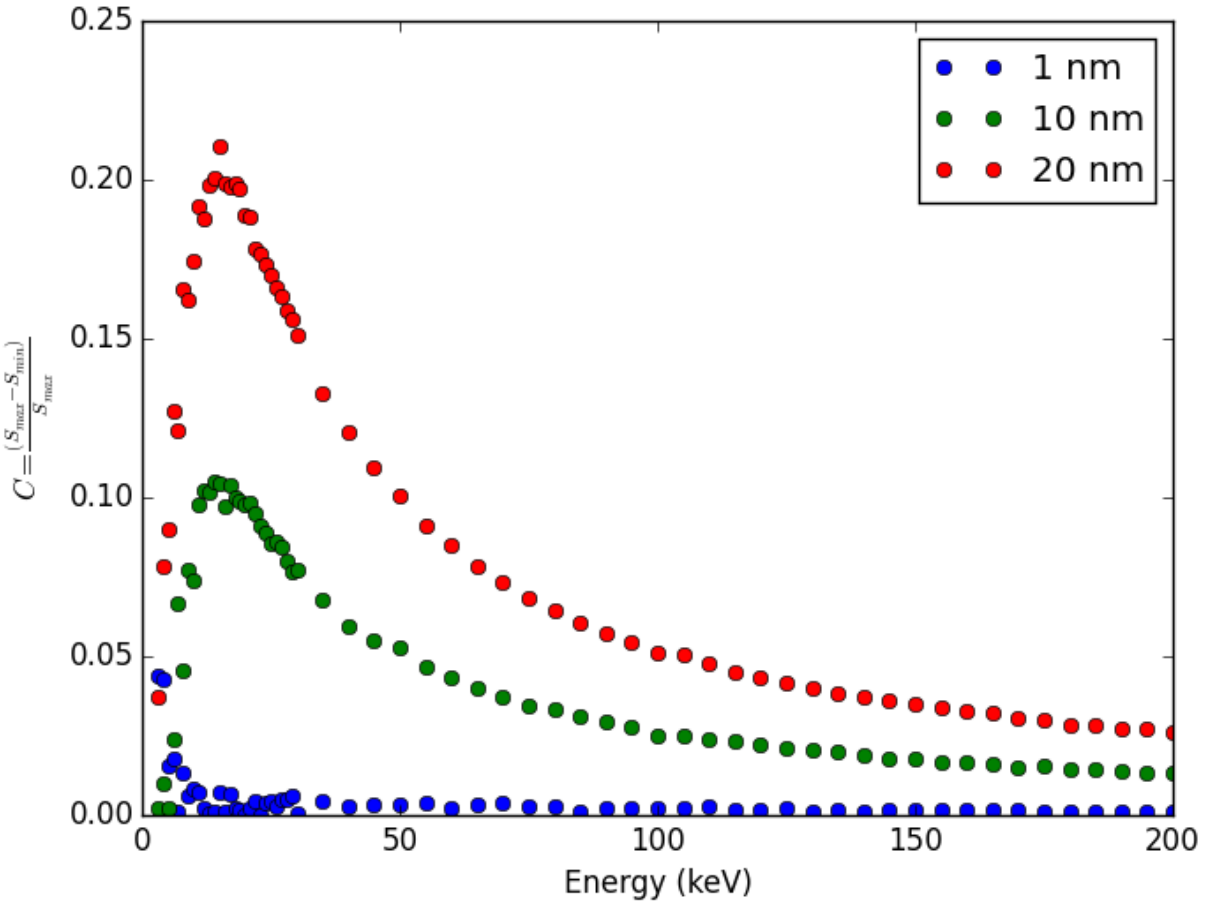

Dislocations in Ti-6Al-4V

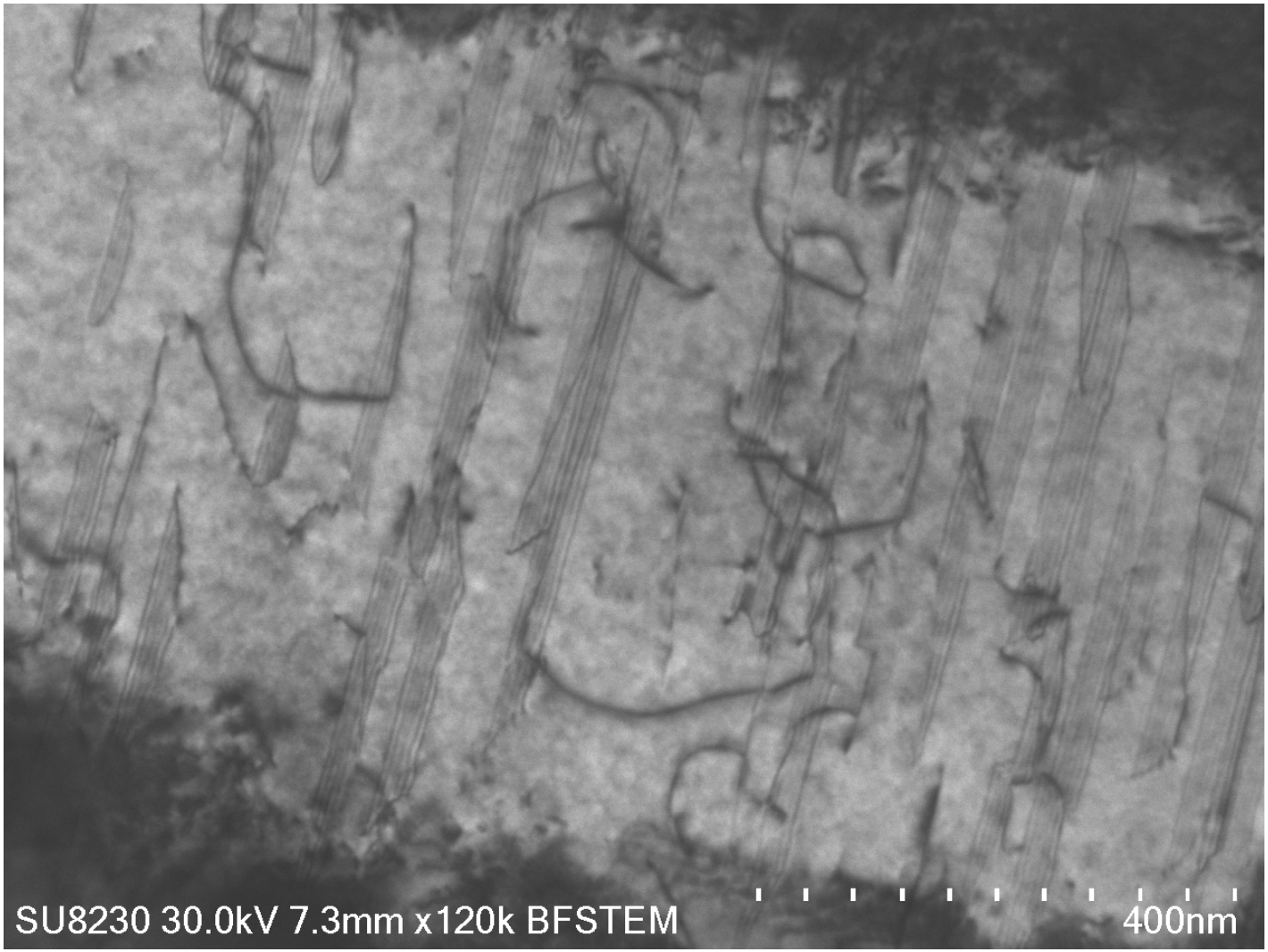

Bruker Flat Quad XFlash 5060F (BFQ)

- Quad detector
  - 4 x 15 mm^2 = 60 mm^2
- Annular design (below objective lens)
- Equipped with Mylar windows
  - Internal window (1 µm)
  - Additional 2 µm or 6 µm windows (on a special changer)
- High count rate capabilities with high collection efficiency

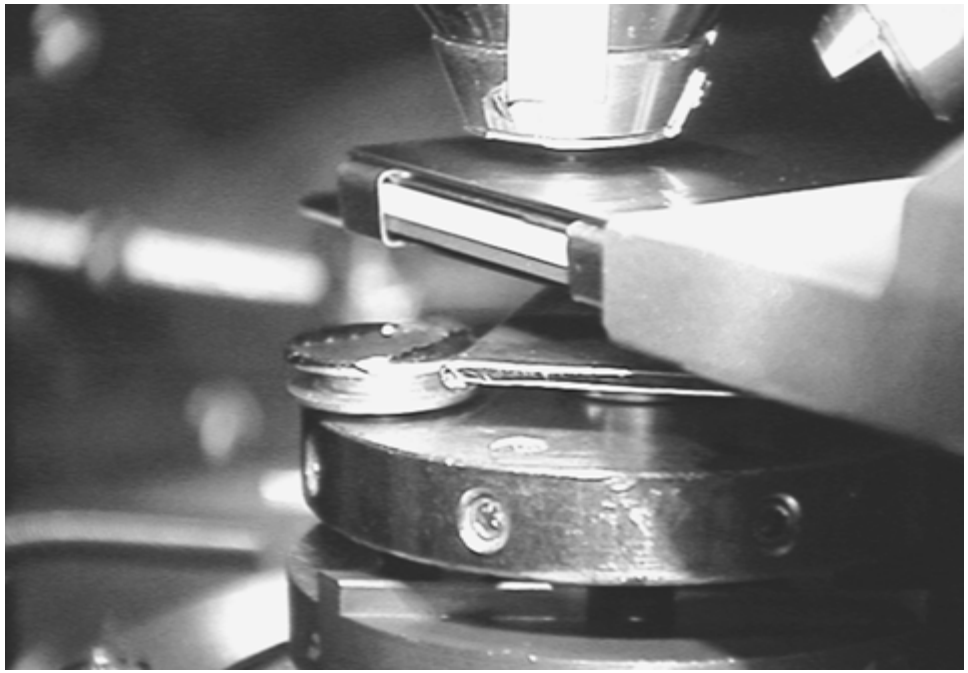

Image from Bruker Nano GmbH.

Pt Particulates on WCNT

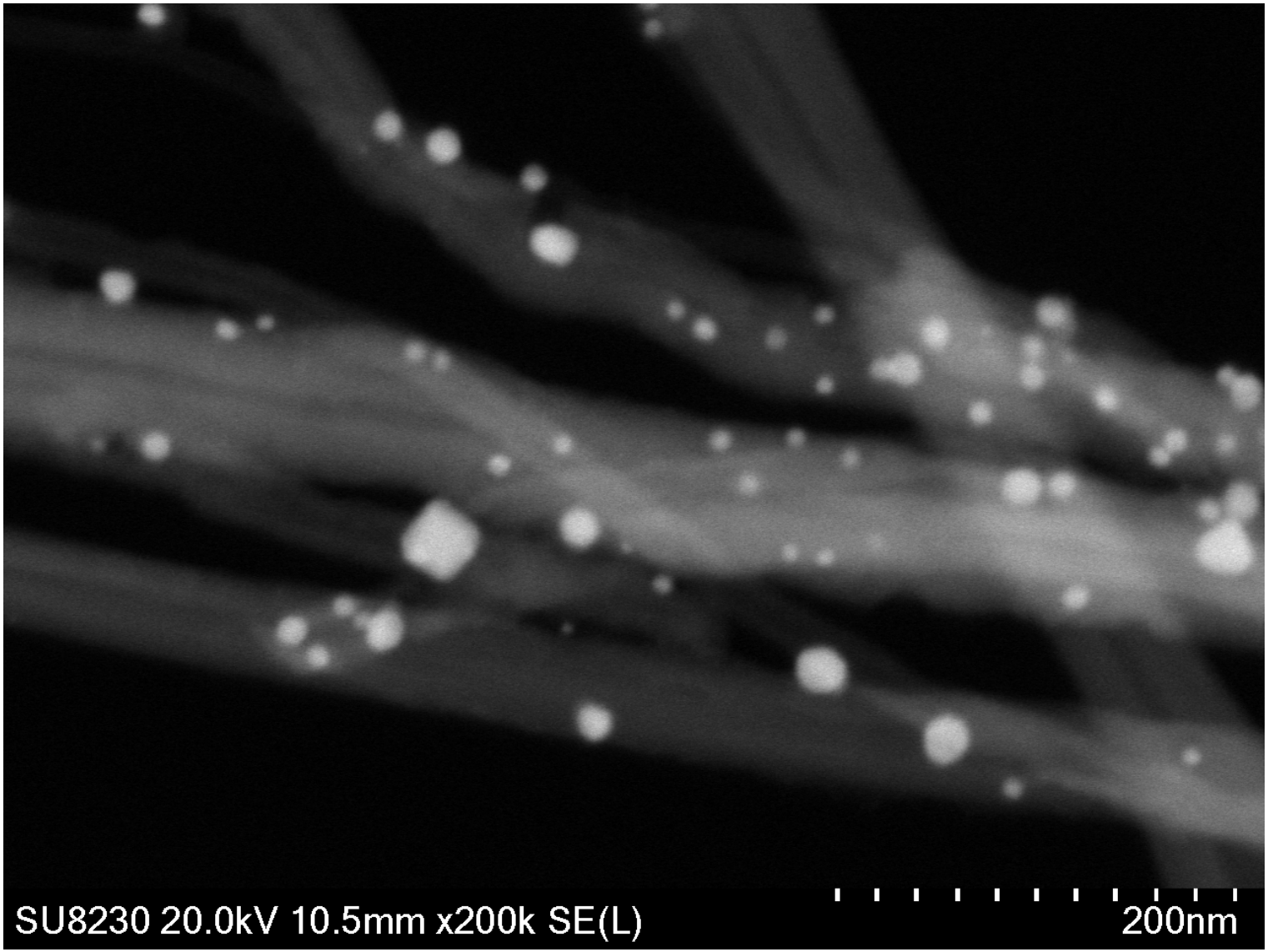

Pt Particulates on WCNT, 7 minutes

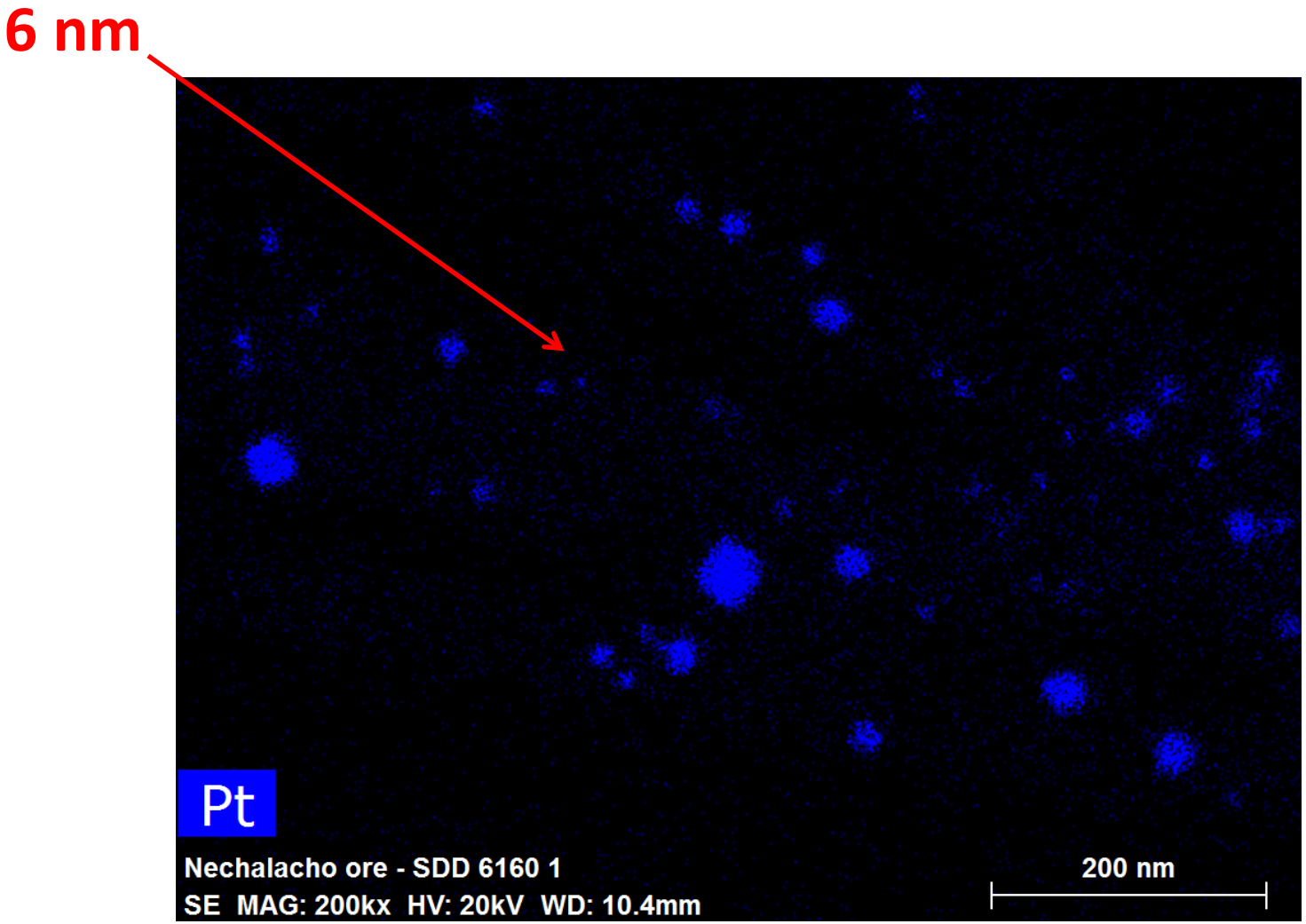

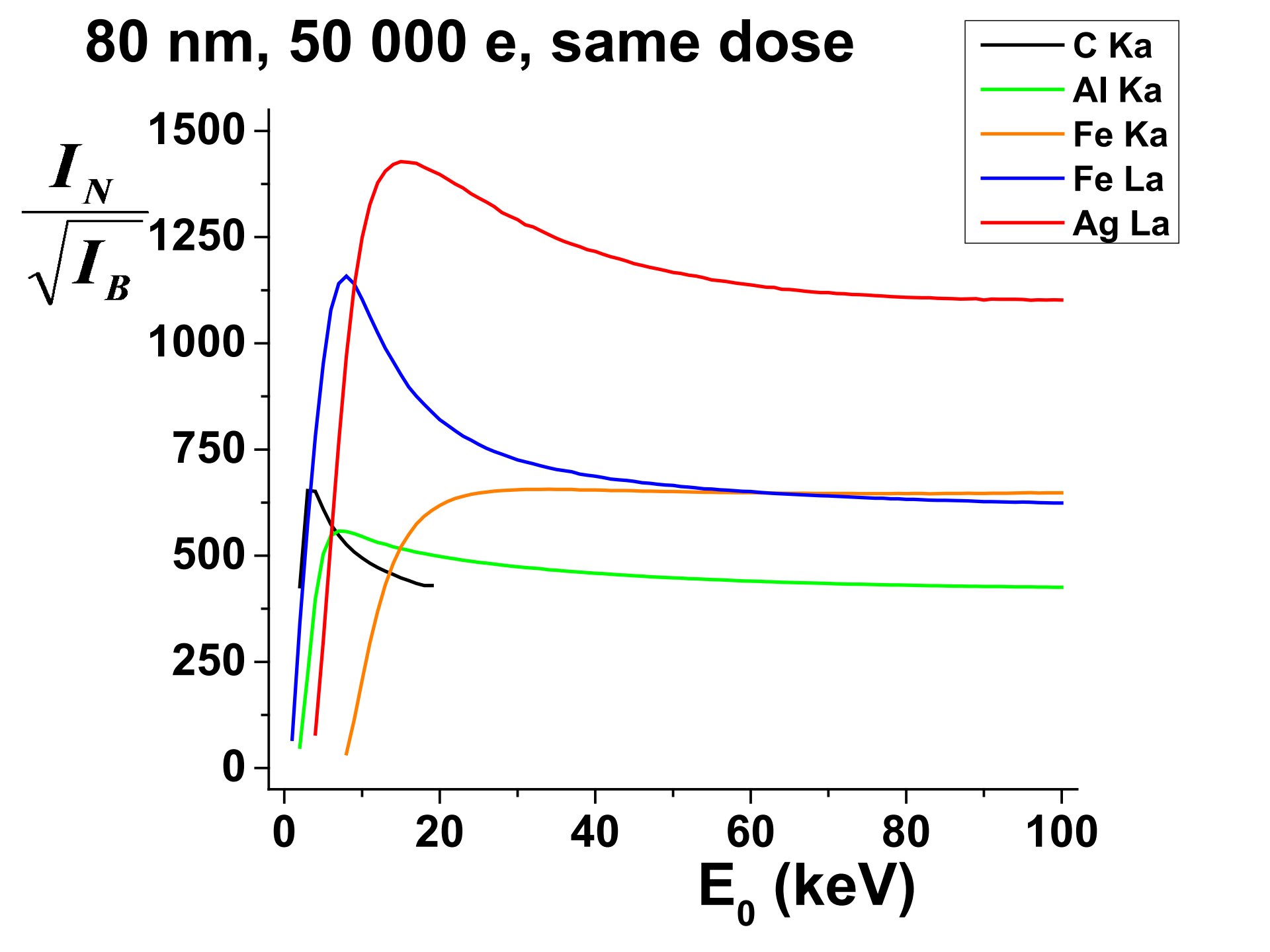
80 nm, 50 000 e, same dose
C Ka
Al Ka
Fe Ka
Fe La
Ag La
$\frac{I_N}{\sqrt{I_B}}$
1500
1250
1000
750
500
250
0
0
20
40
60
80
100
E_0 (keV)

Electron diffraction in the SEM/STEM (semi-immersion type)

- Convergent beam diffraction (on-axis TKD set-up)

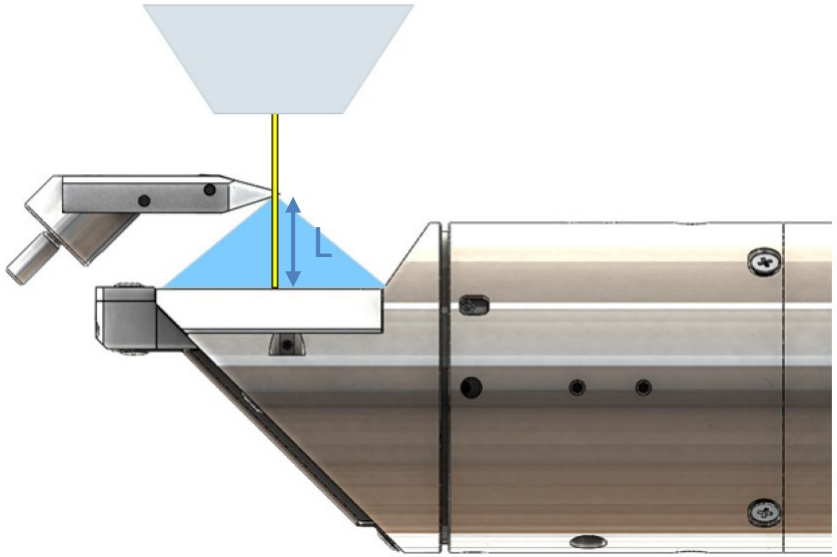

- High sensitivity
- Large collection angle
- Adjustable camera length (L)
- Mapping capability of the EBSD system
- Allows TKD and CBED

Electron diffraction in the SEM/STEM (semi-immersion type)

- Convergent beam diffraction (on-axis TKD set-up)

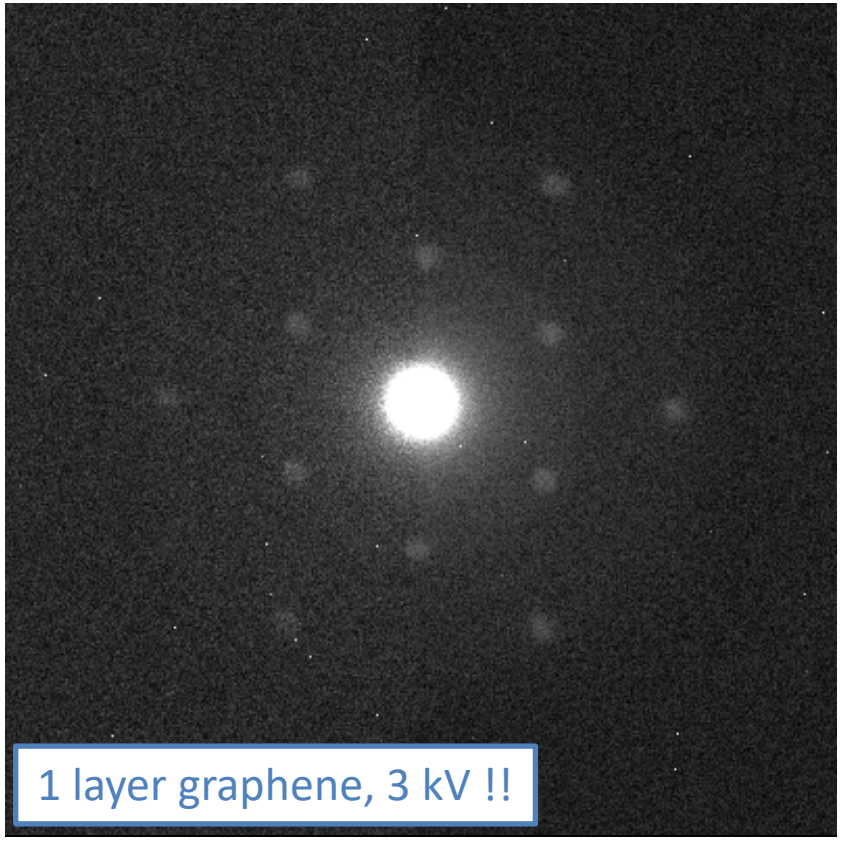

SU-9000EA STEM (2017)

Symmetrical Immersion Lens with Analytical Design

- Small specimen, 3mm or less of radius.
- Small focal length, 3 mm, low aberrations coefficients, smaller probe diameter.
- SE electrons spirals above the lens because of strong magnetic field.
- Highest resolution lens.
- 0.7 Sr Solid Angle for Extreme EDS Detector.

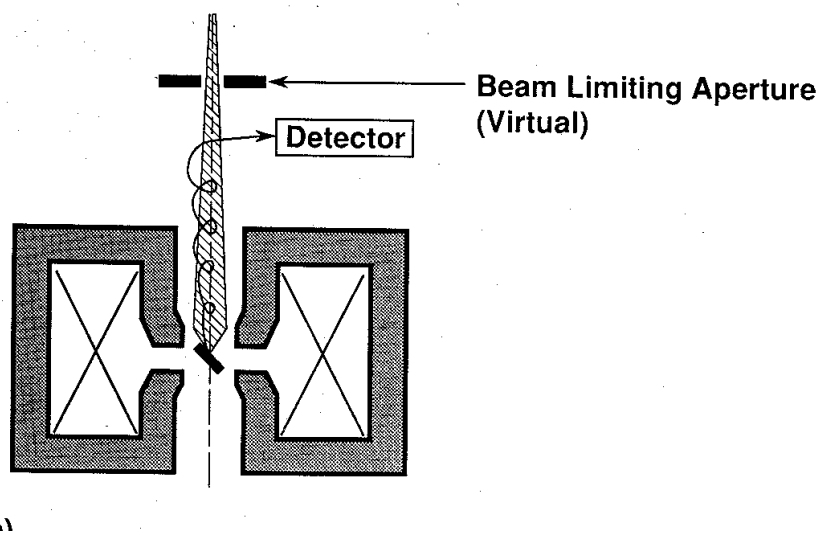

Fe_2O_3 Nanocubes

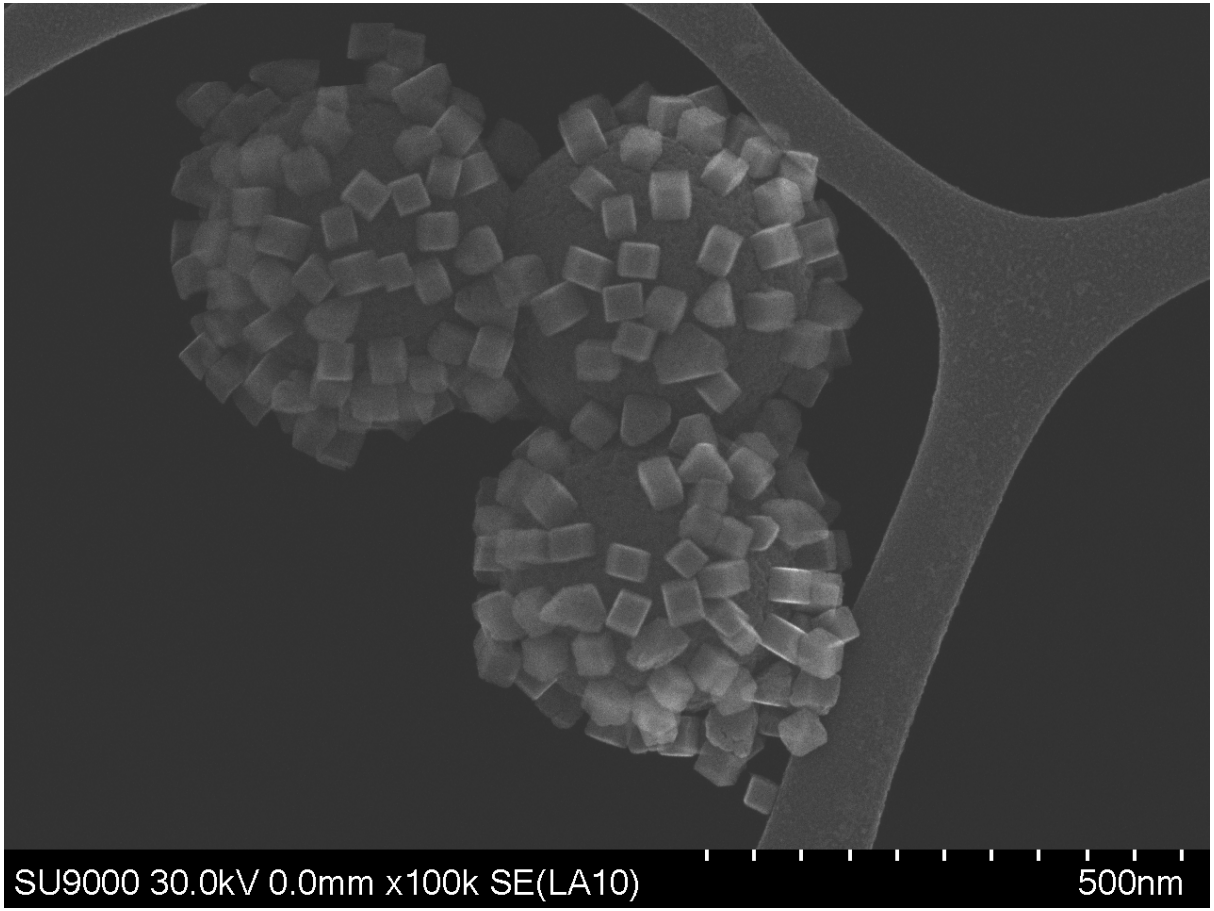

Fe_2O_3 Nanocubes

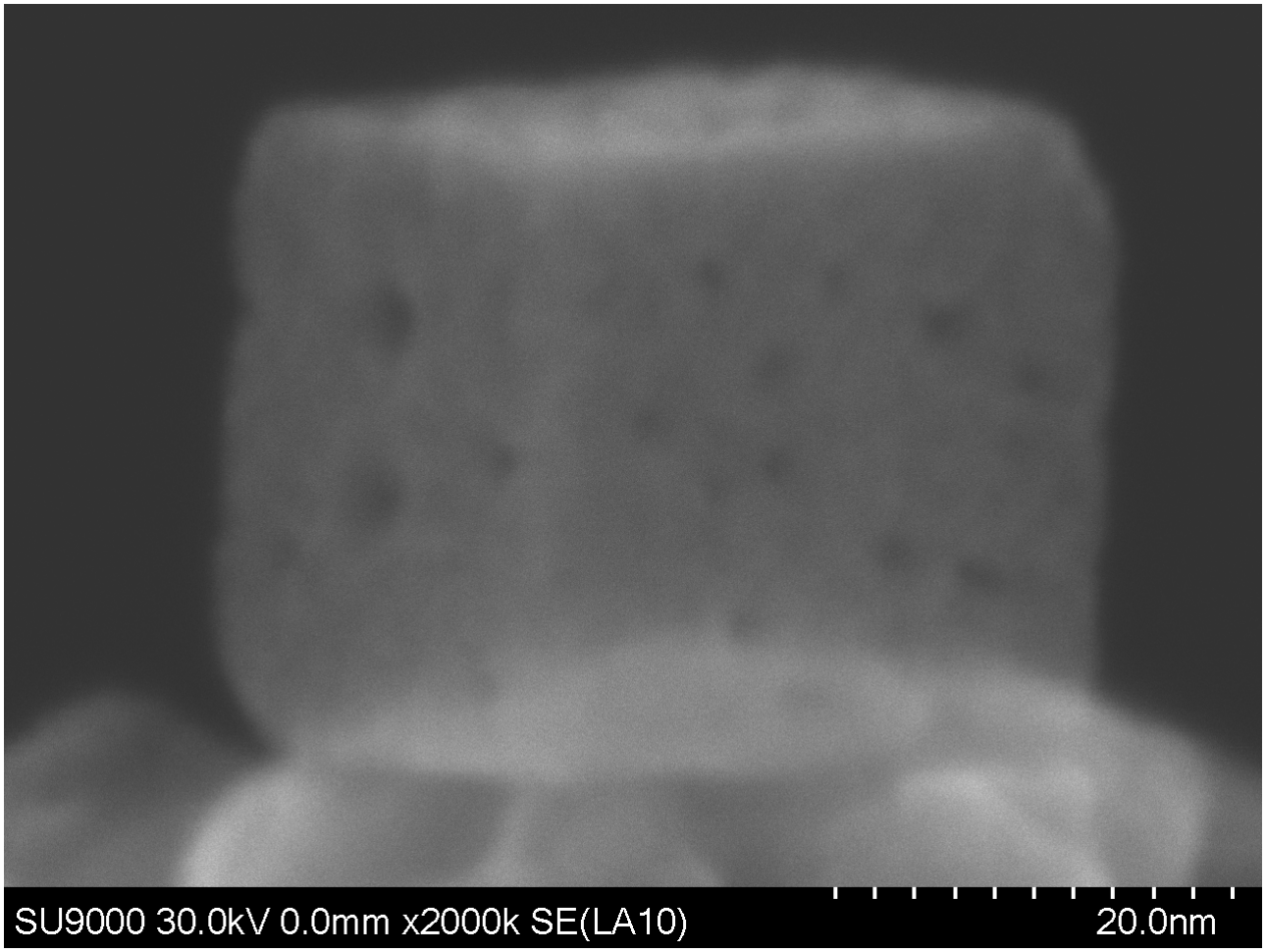

Lattice Imaging of Ni-Pt CNT

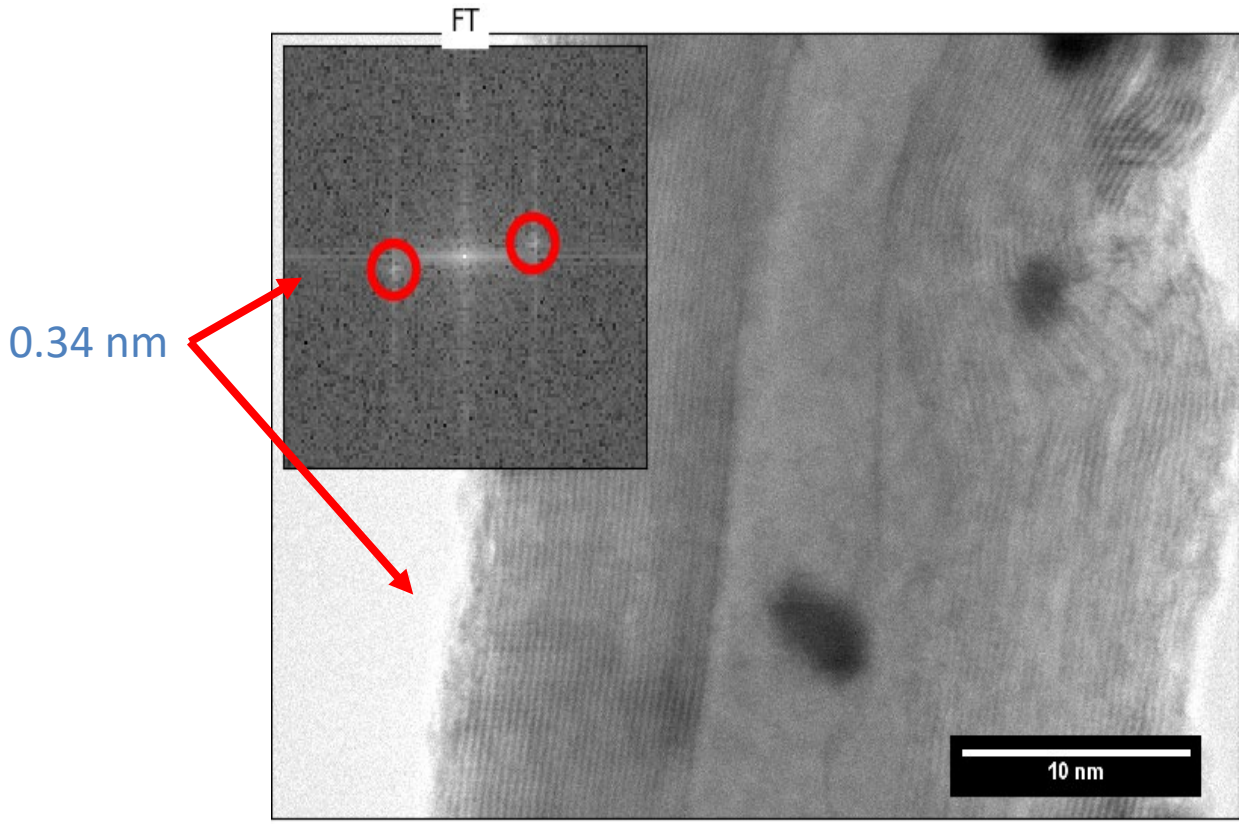

Spatial Resolution with x-rays – 30 kV

- T1 (Al_2CuLi) precipitates in Al-Li-Cu alloys ≈ 1 – 2 nm thick
- 1.6 nm in BF imaging
- 1.9 nm across a T1 precipitate at 30 kV with Cu Kα

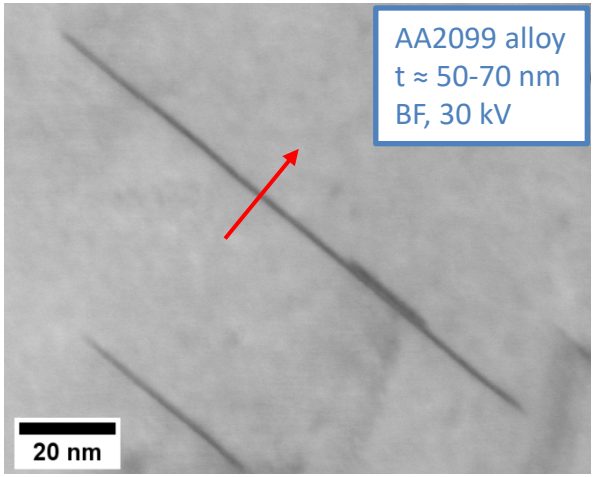

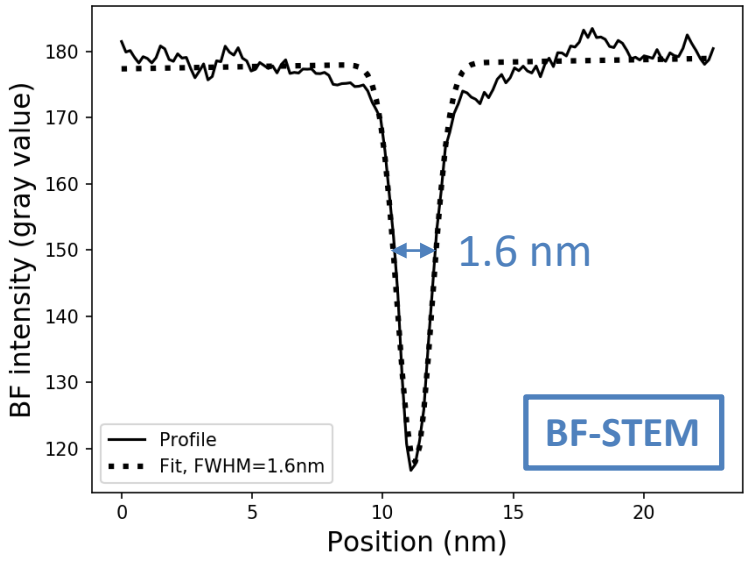

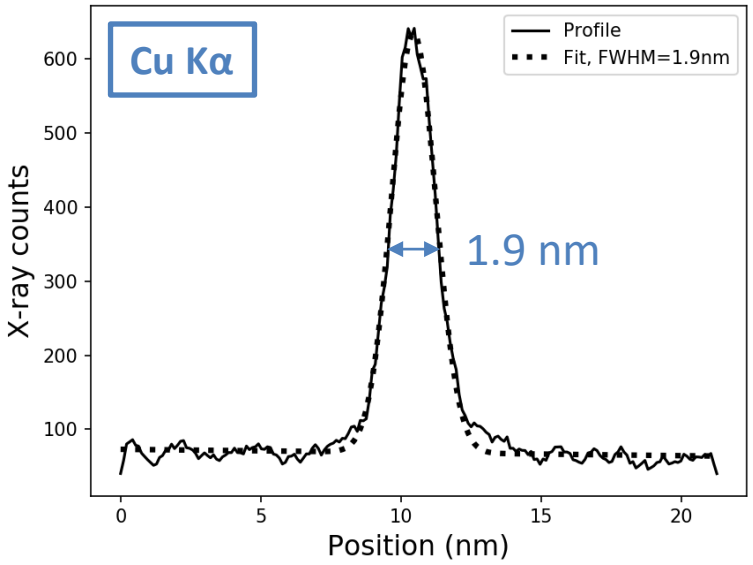

ACS APPLIED NANO MATERIALS

www.acsanm.org Article

Plasmon-Enhanced Hydrogenation of 1-Dodecene and Toluene Using Ruthenium-Coated Gold Nanoparticles

Luis Carlos de la Garza, Nicolas Brodusch, Raynald Gauvin,* and Audrey Moores*

Cite This: *ACS Appl. Nano Mater.* 2021, 4, 1596−1603 Read Online

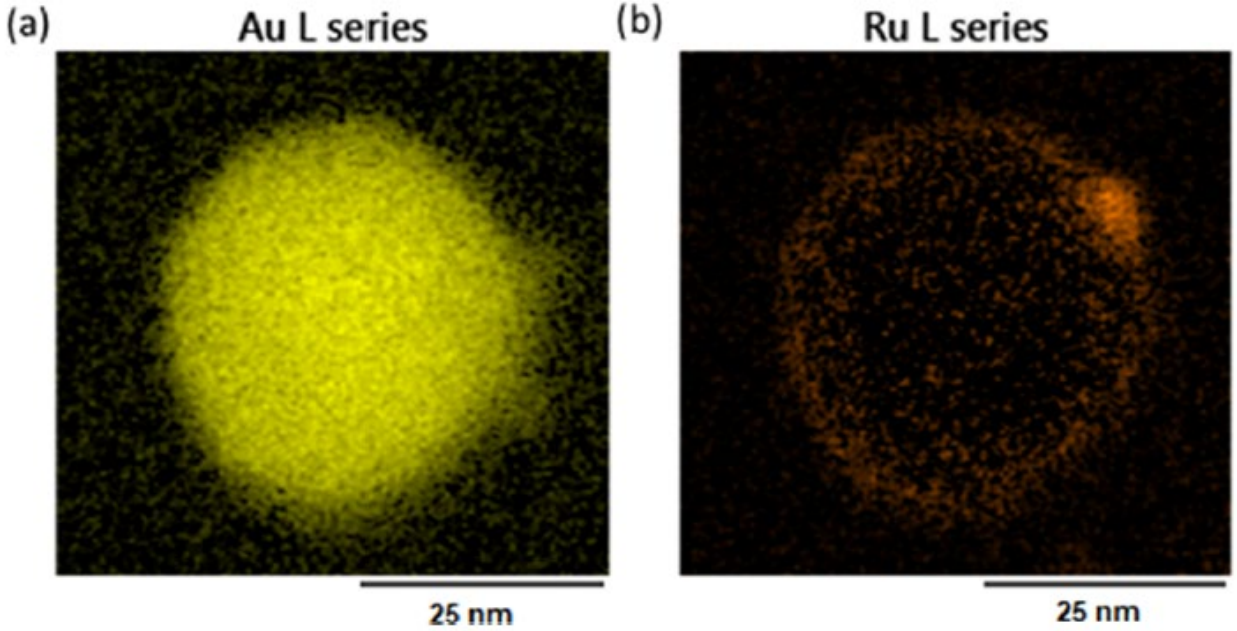

Figure 3. STEM-EDS images of Au@Ru NP. (a) Au L signal, (b) Ru L signal.

SU-9000 - EELS Detector

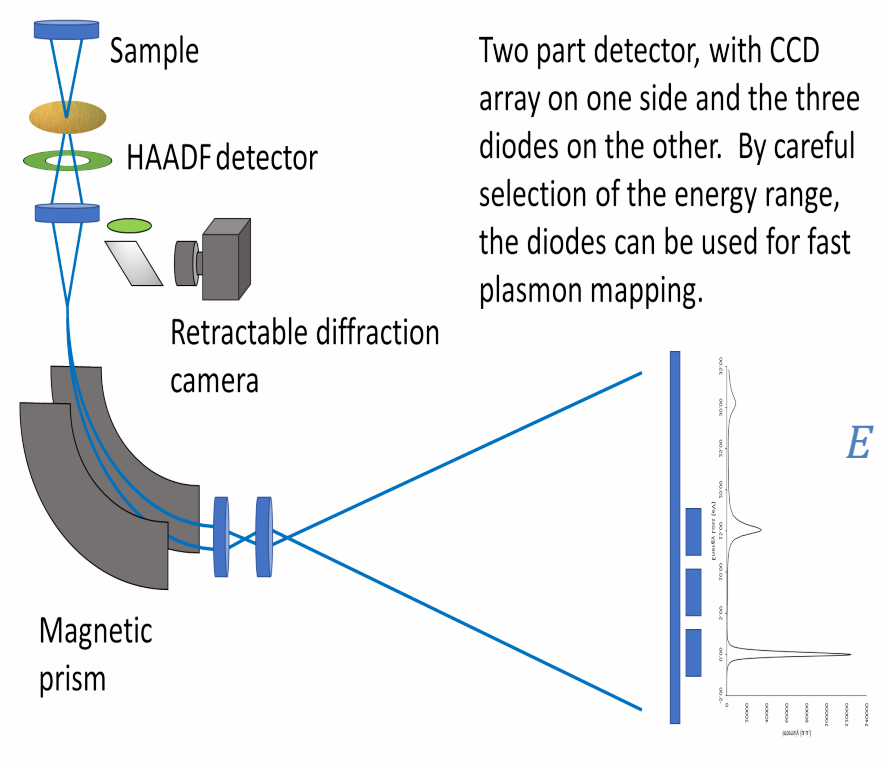

$$r = \frac{mv}{eB}$$

$$E \cong \frac{1}{2}mv^2 \ (E \leq 30\ keV)$$

$$E = mc^2\left(\frac{1}{\sqrt{1-\frac{v^2}{c^2}}} - 1\right)$$

Figure 1: Simplified diagram of the microscope, showing the HAADF detector, the diffraction camera and the dual mode EELS/EF-STEM detector.

AA 2099

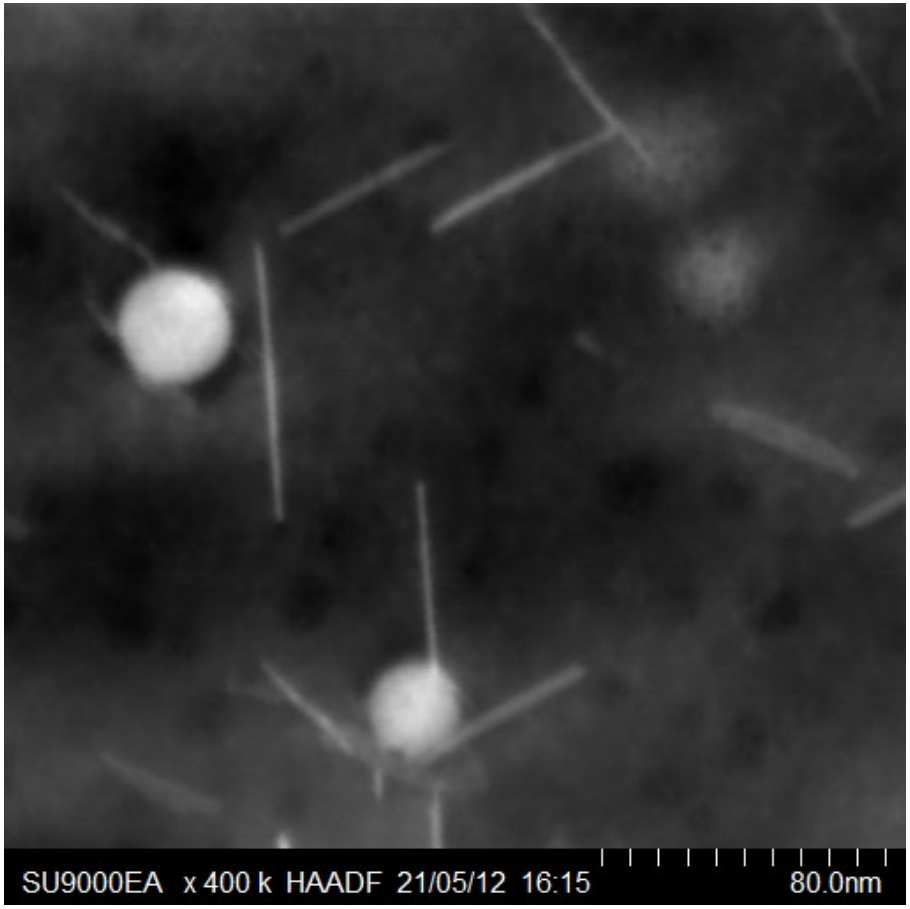

HAADF

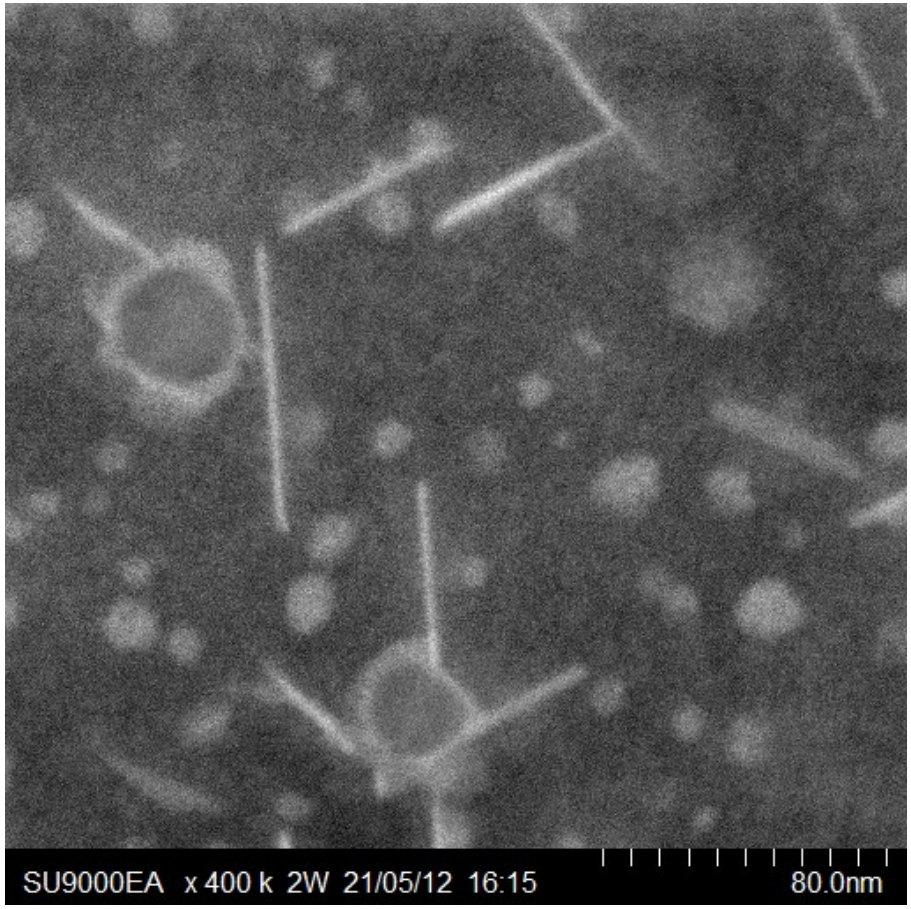

Li Jump Ratio

EELS Lattice Imaging of TiO_2

Surface Plasmon (2)

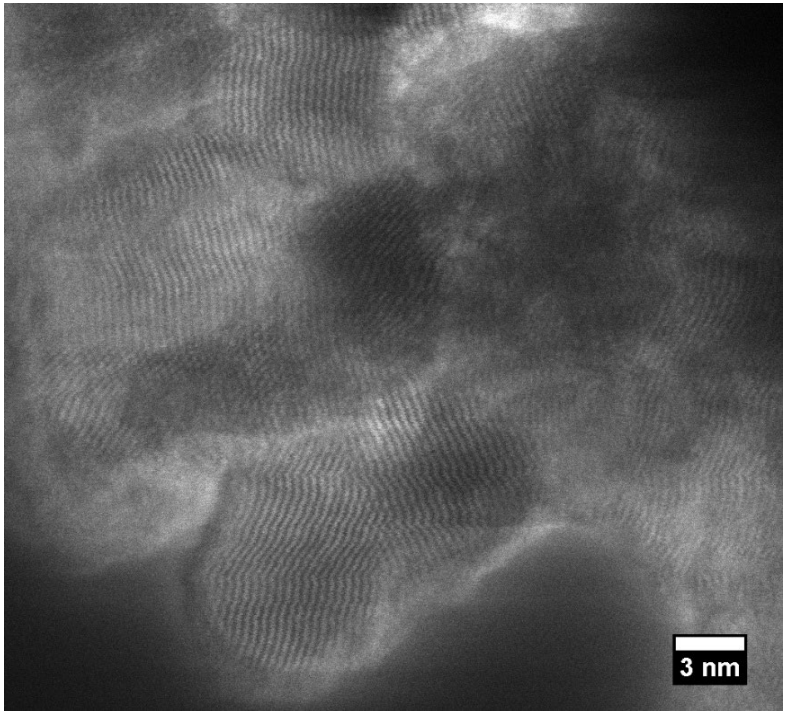

Bulk Plasmon (3)

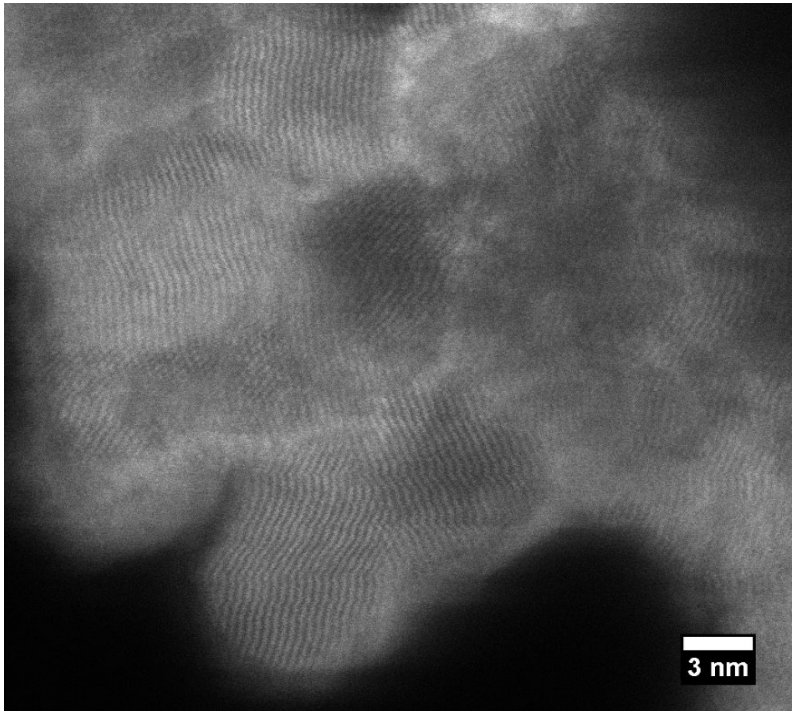

Hitachi Ethos NX-5000 Triple Beam FIB - 2020

First Results FIB
Low C Martensitic Steel. Pr. Yue
100 nm thin film – 30 keV

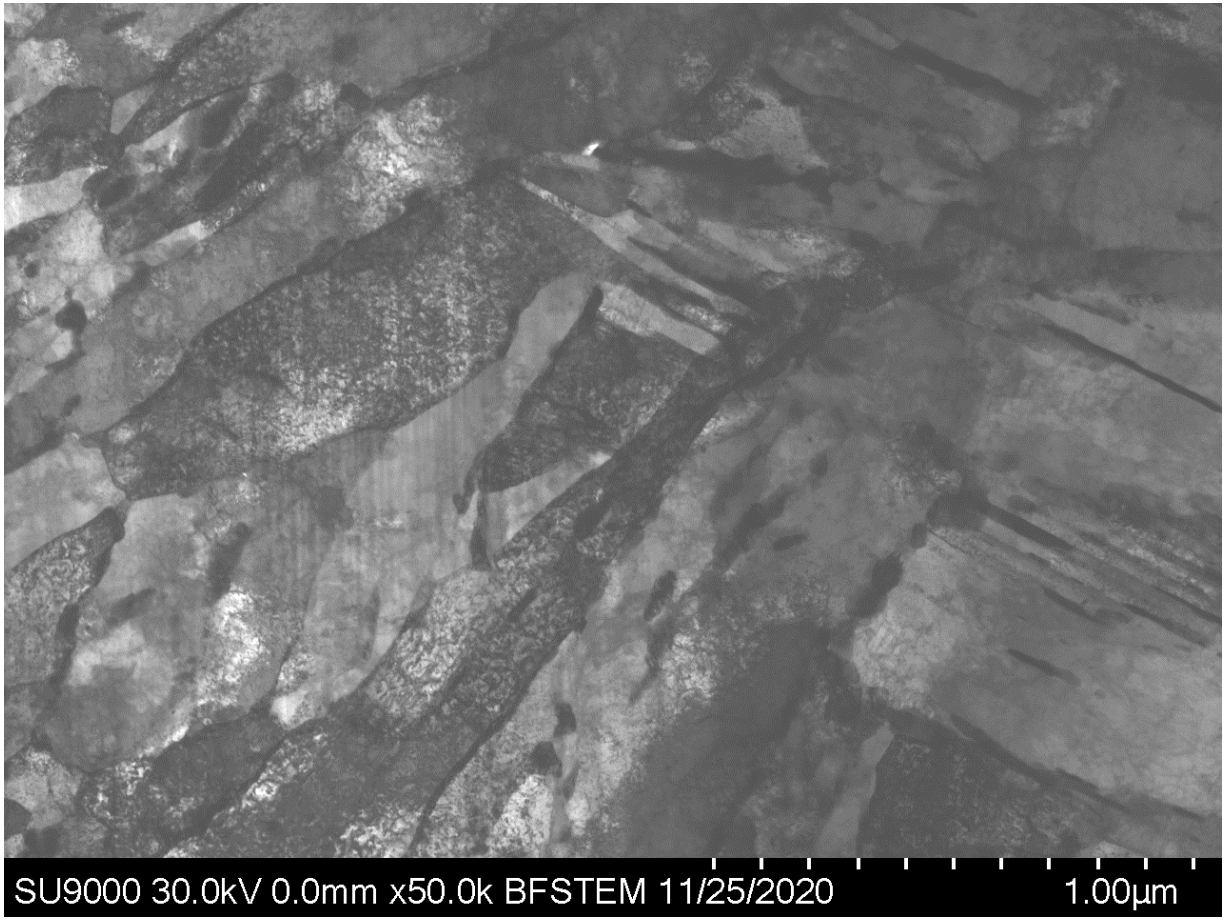

SU – 8230 EBSD in Transmission

TKD map on low carbon martensitic steel
(T. Das / S. Yue)

DF (colorized)

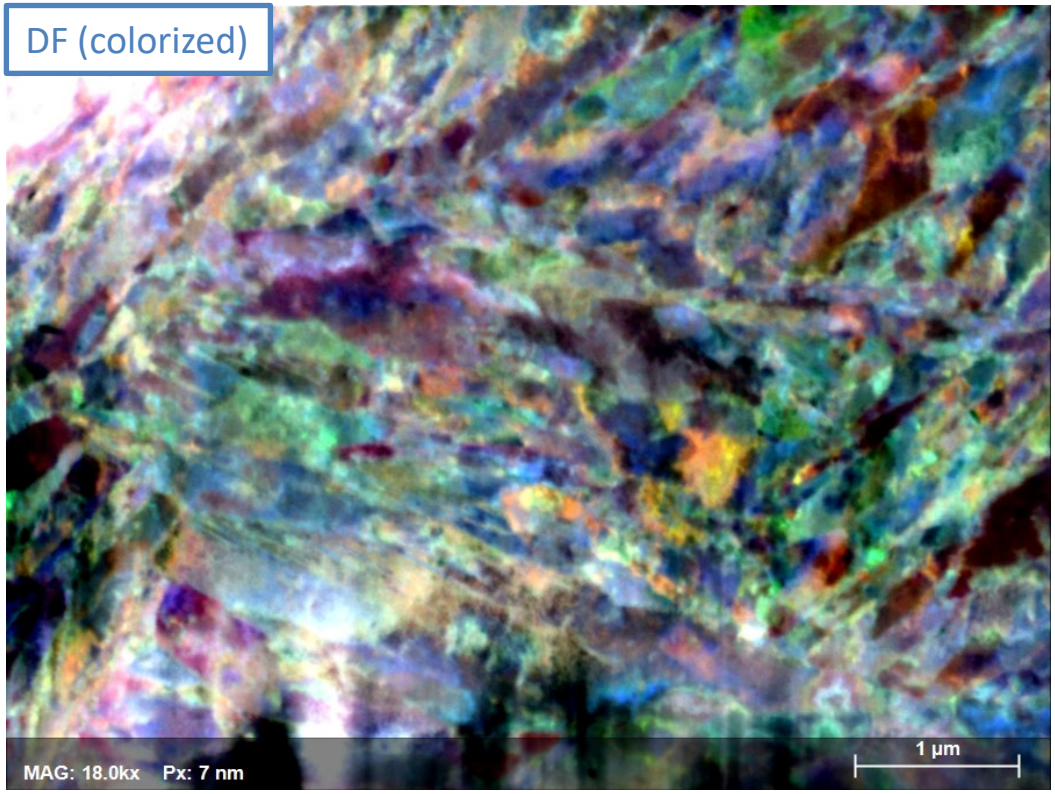

Band contrast map

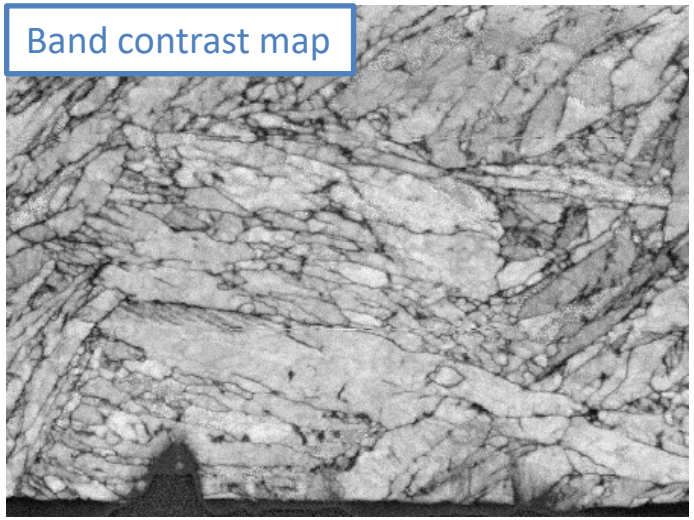

Grain map

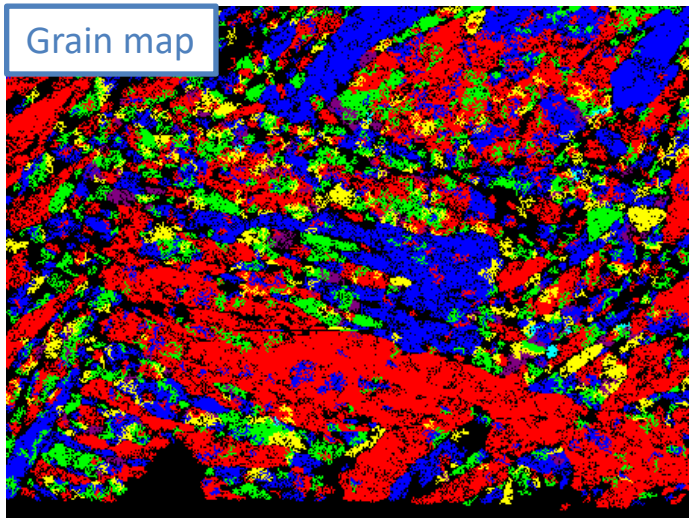

Smallest grains 10 – 15 nm

30 keV, D = 1 nm , t = 80 nm, 5 Me

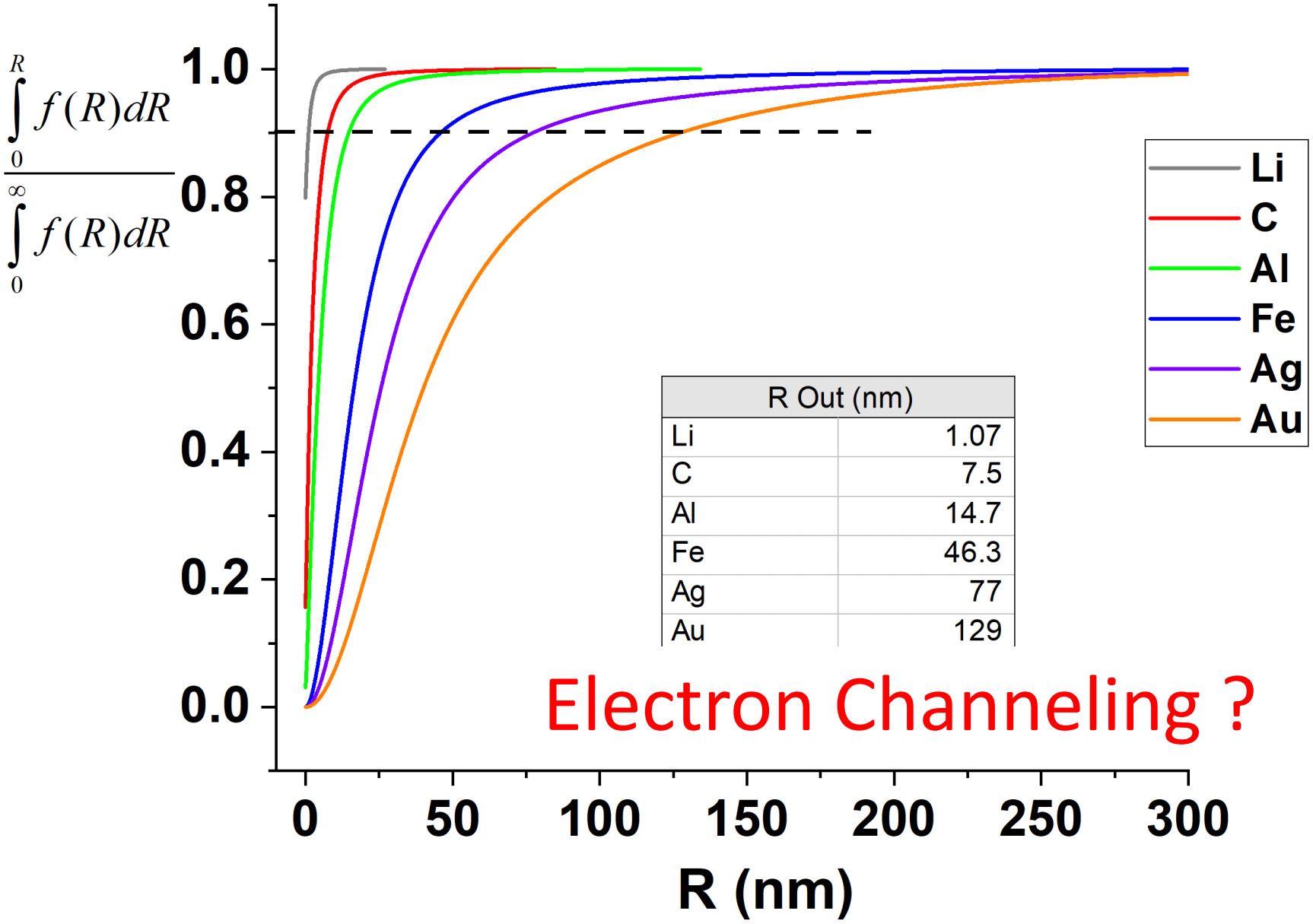

R Out (nm)	
Li	1.07
C	7.5
Al	14.7
Fe	46.3
Ag	77
Au	129

Electron Channeling ?

Si FIB lamella

SU9000 at 30keV

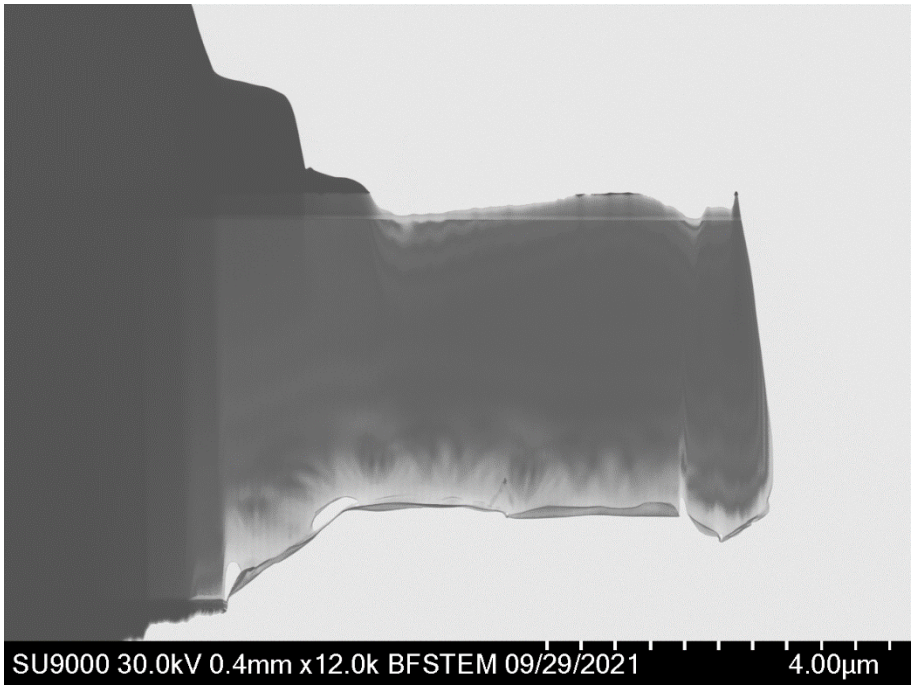

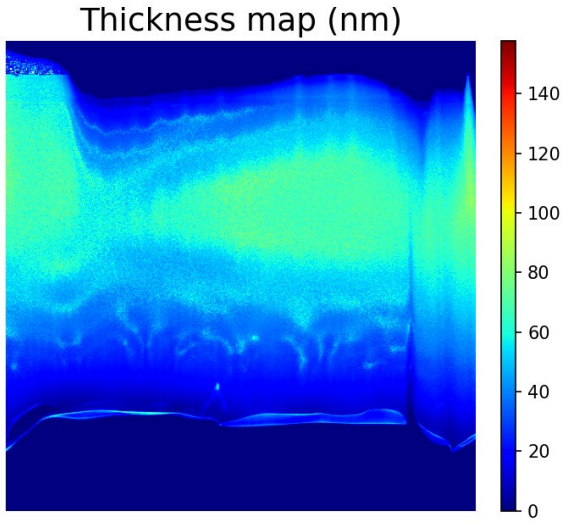

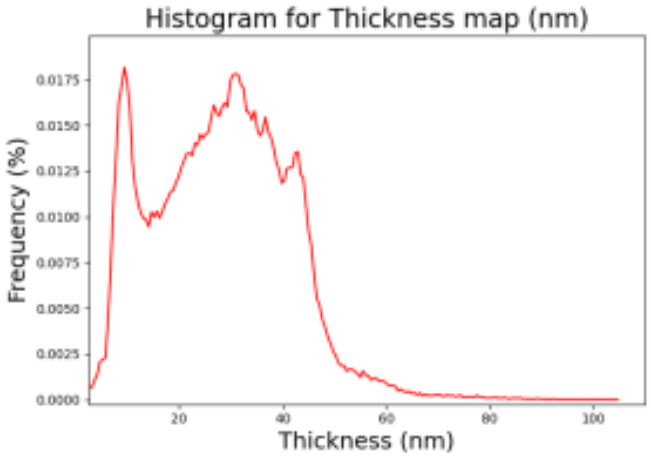

Si, (022) planes, 30 keV

BF

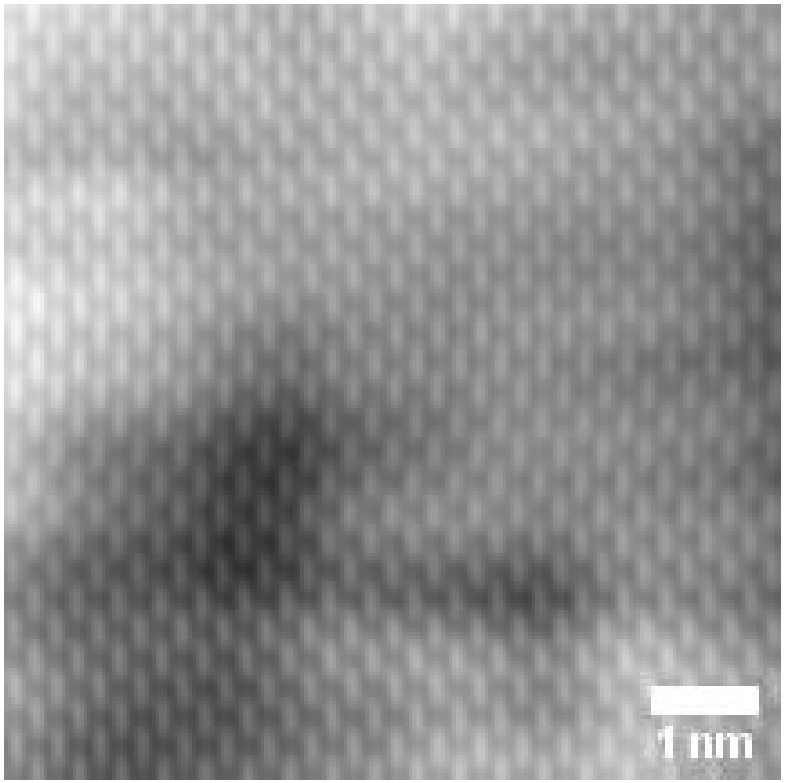

HAADF

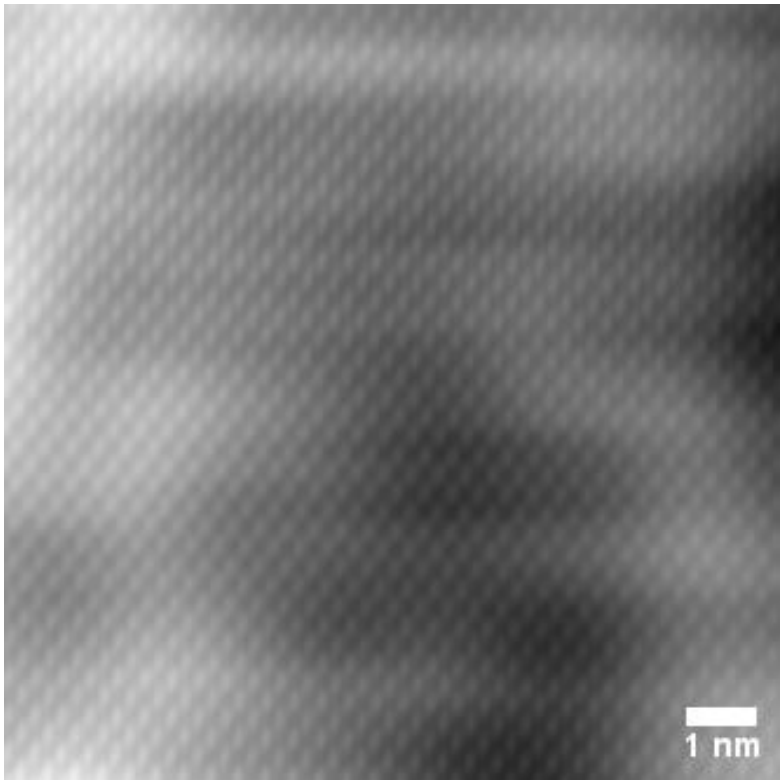

Lattice spacing of 0,19 nm.

Spodumene EELS - 30keV Cryo-holder, 77 K

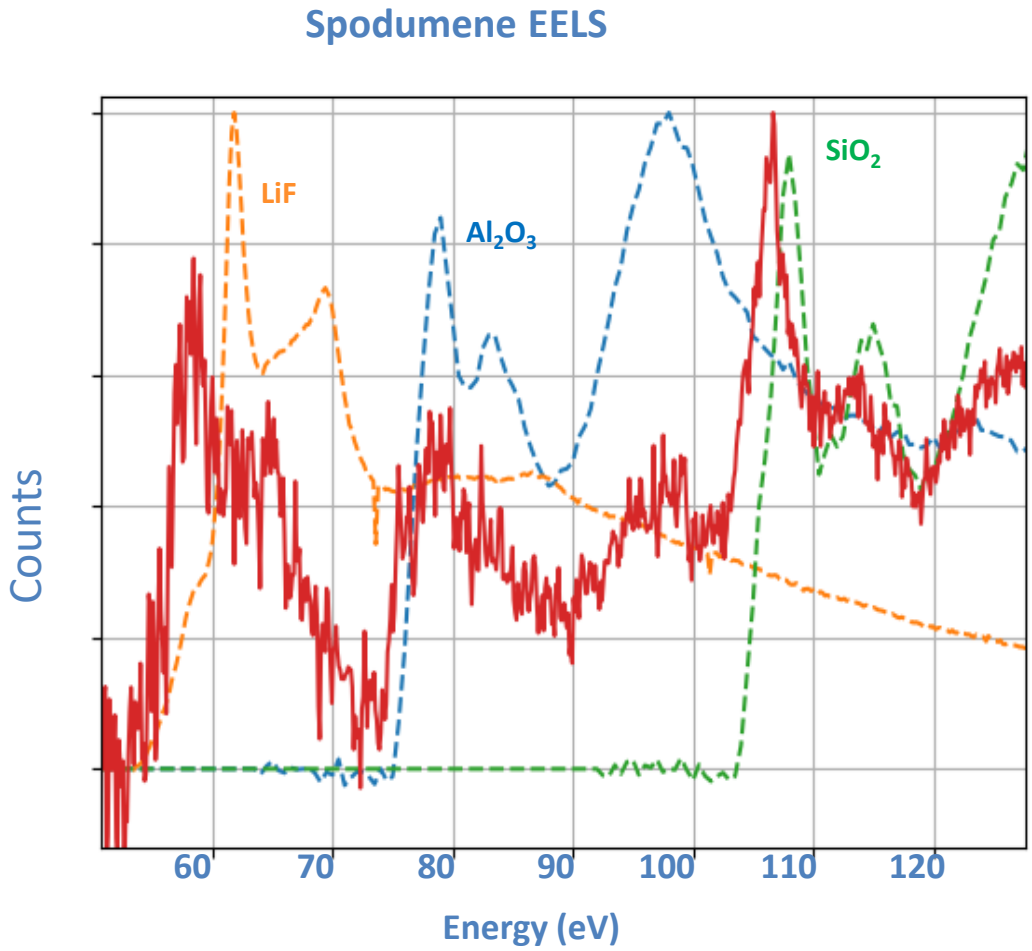

Field Emission Scanning Electron Microscopy
New Perspectives for Materials Characterization

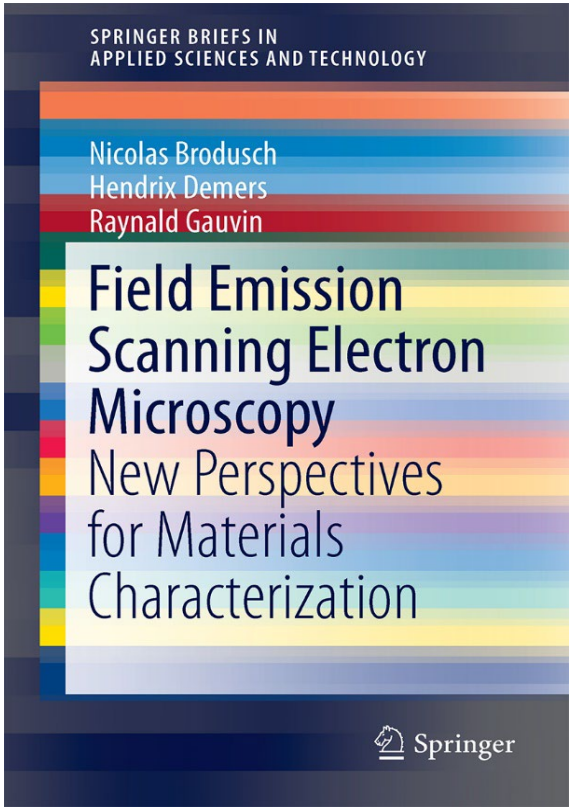

- Authors
  - Nicolas Brodusch
  - Hendrix Demers
  - Raynald Gauvin
- Available now at Springer or Amazon

http://www.springer.com/gp/book/9789811044328

Bas Voltage SEM - STEM

Moins Dispendieux

Plus de temps de microscopie


memrg.com